

VoLTA: Vision-Language Transformer with Weakly-Supervised Local-Feature Alignment

Shraman Pramanick^{*1,2†} Li Jing^{*2} Sayan Nag^{*3} Jiachen Zhu⁴ Hardik Shah²

Yann LeCun^{2,4} Rama Chellappa¹

¹Johns Hopkins University ²Meta ³University of Toronto ⁴New York University

Reviewed on OpenReview: <https://openreview.net/forum?id=Kt2VJrCKo4>

Abstract

Vision-language pre-training (VLP) has recently proven highly effective for various uni- and multi-modal downstream applications. However, most existing end-to-end VLP methods use high-resolution image-text-box data to perform well on fine-grained region-level tasks, such as object detection, segmentation, and referring expression comprehension. Unfortunately, such high-resolution images with accurate bounding box annotations are expensive to collect and use for supervision at scale. In this work, we propose VoLTA (**Vision-Language Transformer with weakly-supervised local-feature Alignment**), a new VLP paradigm that only utilizes image-caption data but achieves fine-grained region-level image understanding, eliminating the need for expensive box annotations. VoLTA adopts graph optimal transport-based weakly-supervised alignment on local image patches and text tokens to germinate an *explicit*, *self-normalized*, and *interpretable* low-level matching criterion. In addition, VoLTA pushes multi-modal fusion deep into the uni-modal backbones during pre-training and removes fusion-specific transformer layers, further reducing memory requirements. Extensive experiments on a wide range of vision- and vision-language downstream tasks demonstrate the effectiveness of VoLTA on fine-grained applications without compromising the coarse-grained downstream performance, often outperforming methods using significantly more caption and box annotations. Code and pre-trained model are available at <https://github.com/ShramanPramanick/VoLTA>.

1 Introduction

Inspired by the escalating unification of transformer-based modeling in vision (Dosovitskiy et al., 2021; Liu et al., 2021; Chen et al., 2021a) and language (Devlin et al., 2019; Liu et al., 2019) domains, coupled with readily available large-scale *image-caption* pair data, vision-language pre-training (VLP) (Lu et al., 2019; Li et al., 2020a; Kim et al., 2021; Kamath et al., 2021; Zhang et al., 2021) has recently been receiving increasing attention. VLP has not only been proven the *de-facto* for several vision-language tasks, but it has also been beneficial for traditional vision-only tasks, such as image classification and object detection. Such wide-range applications of VLP can broadly be categorized into two groups: (*i*) tasks requiring image-level understanding, e.g., image classification, image & text retrieval (Plummer et al., 2015), image captioning (Zhou et al., 2020), visual question answering (Antol et al., 2015), and (*ii*) tasks requiring region-level understanding, e.g., object detection, instance segmentation, and referring expression comprehension (Kazemzadeh et al., 2014; Yu et al., 2016). Most existing VLP methods address only one group of application, leaving the question of a generalizable and unified VL framework under-explored.

Traditional VLP methods with image-level understanding (Li et al., 2021a; Wang et al., 2021b; Dou et al., 2022b) utilize large-scale *image-caption* pair datasets and are commonly trained with image-text contrastive

^{*}Equal technical contribution.

[†]Part of this work was done during an internship at Meta.

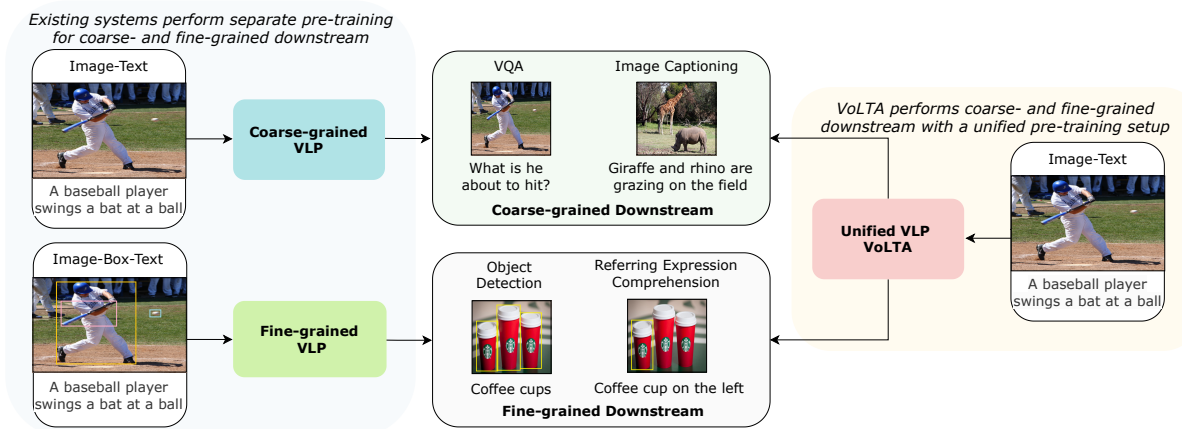


Figure 1: **Different Categories of VLP frameworks.** Existing VLP systems perform separate pre-training for image-level (Li et al., 2021a; Wang et al., 2021b; Dou et al., 2022b) and region-level (Kamath et al., 2021; Li et al., 2022c; Zhang et al., 2022) understanding and do not generalize well to coarse- and fine-grained downstream tasks. In contrast, our proposed method, VoLTA, unifies both downstream with a single pre-training setup and attains fine-grained region-level understanding without using expensive bounding box annotations during pre-training.

objectives computed on global features. Hence, it is not trivial to extend such methods to region-level applications. On the other hand, VLP methods with region-level understanding (Kamath et al., 2021; Li et al., 2022c; Zhang et al., 2022) use *image-text-box* grounding data and are designed to predict bounding boxes during pre-training. Consequently, they do not support image-level tasks. Furthermore, accurate bounding box annotations require high-resolution input images, which are often expensive to collect, annotate and use for pre-training at scale. Recently, FIBER (Dou et al., 2022a) addressed the problem of such unified VLP and proposed a two-stage pre-training algorithm requiring fewer box annotations than previous region-level pre-training methods. Moving a step forward, as shown in Figure 1, we aim to eliminate the use of costly box annotations and ask the challenging but natural question: *Can we attain region-level understanding from global image-caption annotations and unify image- and region-level tasks in a single VL framework?*

Subsequently, we focus on achieving region-level fine-grained understanding by weakly-supervised alignment of image patches and text tokens. Previous VLP methods (Chen et al., 2020d; Kim et al., 2021) in this direction use Wasserstein distance (WD) (Peyré et al., 2019), a.k.a Earth Mover’s distance (EMD)-based optimal transport (OT) algorithms for such alignment problems. However, we argue that WD is not optimum for images with multiple similar entities. Thus, we propose to jointly utilize Gromov-Wasserstein distance (GWD) (Peyré et al., 2016) and Wasserstein distance (WD) in a setup known as graph optimal transport (Chen et al., 2020a). Moreover, instead of using a commonly deployed contrastive objective, we propose to use redundancy reduction from Barlow Twins (Zbontar et al., 2021), which is less data-intensive and does not require hard-negative mining. We also follow Dou et al. (2022a) and incorporate deep multi-modal fusion into the uni-modal backbones, removing the need for costly fusion-specific transformer layers. These steps when integrated yield VoLTA, **Vision-Language Transformer** with weakly-supervised local-feature **A**lignment, a unified VLP paradigm only utilizes *image-caption* annotations but achieves fine-grained region-level image understanding, eliminating the need for expensive box annotations. Figure 4 visualizes the feature-level image-text alignment generated by VoLTA, which can attend text tokens to the corresponding visual patches without relying on low-level supervision.

In summary, our contributions are three-fold. (i) We propose to use graph optimal transport for weakly-supervised feature-level patch-token alignment in VLP. (ii) We introduce VoLTA, a unified VLP paradigm for image-level and region-level applications, but pre-trained only using *image-caption* pairs. VoLTA is memory, compute, and time-efficient and can easily be scaled up with readily available large-scale *image-caption* data harvested from the web. (iii) We present the results of a wide range of vision- and vision-language coarse- and fine-grained downstream experiments to demonstrate the effectiveness of VoLTA compared to strong baselines pre-trained with significantly more caption and box annotations.

2 Related Works

Uni-modal Self-supervised Pre-training: In recent years, the machine learning community has observed a boom in self-supervised pre-training. In the language domain, representations learned by BERT (Devlin et al., 2019), RoBERTa (Liu et al., 2019) have become the default setting for many downstream tasks. Generative models such as GPT (Radford et al., 2019; Brown et al., 2020) have also achieved impressive few-shot/zero-shot performances on novel applications. SimCSE (Gao et al., 2021) uses contrastive learning to help learn useful sentence representations.

In the vision domain, several contrastive/joint-embedding methods (He et al., 2020; Chen et al., 2020c; 2021b; 2020b; Grill et al., 2020; Chen & He, 2021; Caron et al., 2021; Zbontar et al., 2021; Bardes et al., 2022; Shah et al., 2022; Assran et al., 2022) have outperformed supervised counterparts. Recently, generative models such as BEiT (Bao et al., 2021) and MAE (He et al., 2022) have also achieved impressive performances with much more scalable potential.

Vision-Language Pre-training (VLP): Vision-language pre-training mainly relies on *image-text* pair datasets to learn joint visual-language representations. One line of work is to train separate vision and language encoders and only fuse in the representation space. CLIP (Radford et al., 2021), UniCL (Yang et al., 2022a), and ALIGN (Jia et al., 2021) use the image-text contrastive loss to learn aligned representations. SLIP (Mu et al., 2021) combines self-supervised visual representation learning and contrastive multi-modal learning. M3AE (Geng et al., 2022), FLAVA (Singh et al., 2022) combines masked image modeling and masked language modeling. Another line of work uses cross attention to fuse vision and language information in the early stage (Kamath et al., 2021; Dou et al., 2022b; Lu et al., 2019; Li et al., 2020b; Kiela et al., 2019; Kim et al., 2021; Zhang et al., 2021; Li et al., 2022b; Wang et al., 2022c; Pramanick et al., 2023; Park & Han, 2023; Li et al., 2023a; Jang et al., 2023; Wang et al., 2023a). These works focus on learning semantic-level aligned vision-language representations. In addition, UniTAB (Yang et al., 2022c), OFA (Wang et al., 2022b), GLIP (Li et al., 2022c), and FIBER (Dou et al., 2022a) use expensive grounding *image-text-box* annotations to learn the fine-grained aligned representations. Our work uses representation space alignment and cross-attention fusion, but we do not use any box annotation to learn robust feature-level alignments.

Unsupervised Representation Alignment: Unsupervised multi-modal alignment typically relies on specific metrics. Wasserstein distance (Peyré et al., 2019), a.k.a EMD-based optimal transport (OT) algorithms have been widely adopted to various domain alignment tasks, including sequence-to-sequence learning (Chen et al., 2019), few-shot learning (Zhang et al., 2020), knowledge distillation (Balaji et al., 2019), unsupervised domain adaptation (Balaji et al., 2019), generative networks (Han et al., 2015; Genevay et al., 2018; Mroueh et al., 2018; 2019), and multi-modal learning (Yuan et al., 2020; Chen et al., 2020d; Kim et al., 2021; Li et al., 2022d; Pramanick et al., 2022). Previous VLP methods (Chen et al., 2020d; Kim et al., 2021), which use OT-based patch-word alignment, only utilize the Wasserstein distance. However, we argue that jointly modeling GWD (Peyré et al., 2016) and WD results in a superior multi-modal alignment for intricate images. To the best of our knowledge, this is the first work to apply WD and GWD-based optimal transport for feature-level alignment in VLP.

3 Proposed System - VoLTA

In this section, we present our proposed approach, VoLTA, which contains three broad modules - *(i)* intra- and inter-modality redundancy reduction, *(ii)* weekly-supervised cross-modal alignment of local features, and *(iii)* cross-modal attention fusion (CMAF). Next, we introduce the fine-tuning strategies for various uni- and multi-modal downstream tasks as supported by VoLTA. An overview of the different modules of VoLTA is presented in Figure 2.

3.1 Intra- & Inter-modality Redundancy Reduction

We use Barlow Twins (BT) (Zbontar et al., 2021), a non-contrastive covariance regularization as the foundational objective of VoLTA. The recent success of contrastive vision-language pre-training (Radford et al., 2021; Li et al., 2021b; Jia et al., 2021; Kim et al., 2021; Yang et al., 2022a; Dou et al., 2022a;b) has already

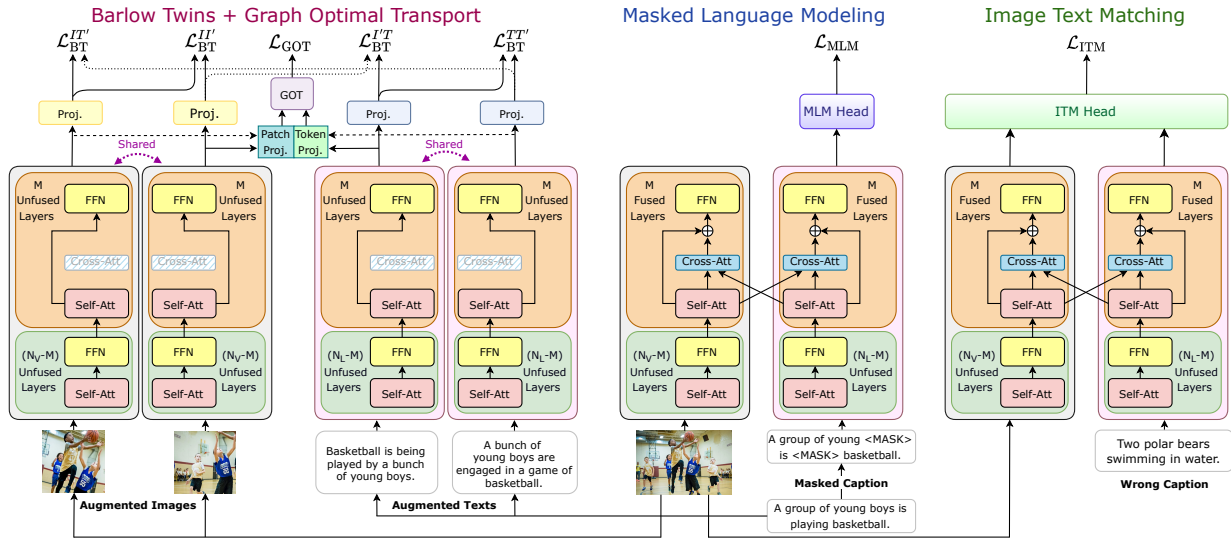


Figure 2: **Computation of four different objectives, \mathcal{L}_{BT} , \mathcal{L}_{GOT} , \mathcal{L}_{MLM} , and \mathcal{L}_{ITM} by the proposed VoLTA framework.** Inspired by Dou et al. (2022a), VoLTA inserts cross-modal attention fusion (CMAF) inside uni-modal backbones with a gating mechanism. During VoLTA pre-training, every forward iteration consists of three steps - (i) CMAF is switched off, VoLTA acts as dual encoder, \mathcal{L}_{BT} and \mathcal{L}_{GOT} are computed. (ii) CMAF is switched on, VoLTA acts as fusion encoder, and image-masked caption pair is fed into the model to compute \mathcal{L}_{MLM} . (iii) CMAF is kept on, randomly sampled image-caption pair is fed into the model to compute \mathcal{L}_{ITM} . Such a fusion strategy results in a lightweight and flexible model compared to using fusion-specific transformer layers.

shown that, compared to a single modality, *image-caption* pairs offer a significantly higher-level of abstractive and semantic concepts about the training samples. However, common contrastive VLP objectives, like InfoNCE (Oord et al., 2018), are data-hungry, as they require large batch sizes and well-mined hard negatives. On the other hand, the BT objective operates on the dimensions of the embeddings across the two views of training samples. Hence, it is more robust to batch size and can be trained using lower memory resources. In this work, we extend the BT objective for a multi-modal setup.

The original BT algorithm, which operates on joint embeddings of distorted samples, was proposed only for image modality. Specifically, for each image of a batch \mathcal{X} , two distorted views are obtained using a distribution of data augmentation \mathcal{T} with disparate probabilities. These distorted images are then fed into a shared image encoder containing a feature extraction network (e.g., ResNet (He et al., 2016)) cascaded with trainable linear projection layers, producing a batch of parallel embeddings z^A and z^B . The BT loss computed using the encoded embeddings can be denoted as:

$$\mathcal{L}_{\text{BT}} \triangleq \sum_i (1 - C_{ii})^2 + \lambda \sum_i \sum_{j \neq i} (C_{ij})^2, \text{ where, } C_{ij} = \frac{\sum_b z_{b,i}^A z_{b,j}^B}{\sqrt{\sum_b (z_{b,i}^A)^2} \sqrt{\sum_b (z_{b,j}^B)^2}} \quad (1)$$

λ is a positive weighting factor; C is the cross-correlation matrix computed between z^A and z^B along the batch dimension; b stands for sample indices in a batch; i, j refers to the dimension indices of z^A and z^B . The first term in Equation 1 is the *invariance* term which attempts to equate the diagonal elements of the cross-correlation C matrix to 1, whereas the second term is the *redundancy reduction term* which pushes the off-diagonal elements of C matrix to 0.

In this work, we use BT for *image-caption* pairs. Specifically, we use stochastic data augmentations for both images and text¹, and directly apply the BT objective for all the 2×2 pairs, resulting in additional supervision. Note this simple, straightforward, and instinctive extension enables us to apply redundancy reduction in between and across modalities, which intuitively results in superior visual representation. Moreover, in this

¹Augmentation details are provided in Appendix D.1.

bi-modal setting, we can pre-train a text encoder in parallel with the image encoder and, thus, can generalize our system to a broader range of uni- and multi-modal downstream applications.

Intra-modal Objective: Intra-modal objective refers to applying the BT loss in-between pairs of image and text embeddings. Given an *image-caption* pair, we first have two augmented views (I, I') for each image, and two augmented views (T, T') for each text. Then, we resort to Equation 1 individually for the image and text pairs.

$$\mathcal{L}_{\text{BT}}^k \triangleq \sum_i (1 - C_{ii}^k)^2 + \lambda \sum_i \sum_{j \neq i} (C_{ij}^k)^2, \forall k \in \{II', TT'\} \quad (2)$$

Inter-modal Objective: Inter-modal objective refers to applying the BT loss across image and text embeddings. Since the image and text encoders can output features with different shapes, we design the projector layers with same output dimension. Hence, in addition to the original BT loss between (I, I') in [Zbontar et al. \(2021\)](#), we get three more loss terms - (T, T') , (I, T') , (I', T) , leading to $3 \times$ diverse and high-quality additional supervision. The inter-modal BT losses can be directly computed following Equation 1.

$$\mathcal{L}_{\text{BT}}^k \triangleq \sum_i (1 - C_{ii}^k)^2 + \lambda \sum_i \sum_{j \neq i} (C_{ij}^k)^2, \forall k \in \{IT', I'T\} \quad (3)$$

The resulting bi-modal BT loss is $\mathcal{L}_{\text{BT}} = \sum_k \mathcal{L}_{\text{BT}}^k, \forall k \in \{II', TT', IT', I'T\}$.

3.2 Alignment of Local Features

Though the inter-modal redundancy reduction provides high-quality semantic supervision, it is computed on the global image- and text features and, thus, only simulates implicit and non-interpretable multi-modal alignment. However, fine-grained region-level downstream applications like detection, segmentation, and reference expression comprehension require local visual feature descriptors with specific spatial information. To achieve this, most existing top-performing VLP methods, including UniTAB ([Yang et al., 2022c](#)), OFA ([Wang et al., 2022b](#)), GLIP ([Li et al., 2022c](#)), and FIBER ([Dou et al., 2022a](#)), use high-resolution image-text-box data for fine-grained pre-training. However, bounding box annotations are expensive to collect and use for supervision. Hence, we seek an alternate weakly-supervised solution for local feature-level alignment using global image-caption annotations.

Recently, WD ([Peyré et al., 2019](#)), a.k.a EMD-based OT algorithms have been used for weakly-supervised patch-word alignment in VLP ([Chen et al., 2020d; Kim et al., 2021](#)). Such OT-based learning methods are optimized for distribution matching by minimizing the cost of a transport plan. We pose the patch-word alignment as a more structured graph-matching problem and use the graph optimal transport (GOT) algorithm, which utilizes GWD ([Peyré et al., 2016](#)) in conjunction with WD to ensure the preservation of topological information during cross-modal alignment. More specifically, we obtain the patch- and token-level features from the last layers of corresponding visual and textual transformer encoders, and use these encoded local-feature vectors to construct modality-specific dynamic graphs - $\mathcal{G}_x(\mathbb{V}_x, \mathcal{E}_x)$ for image patches and $\mathcal{G}_y(\mathbb{V}_y, \mathcal{E}_y)$ for text tokens. Each

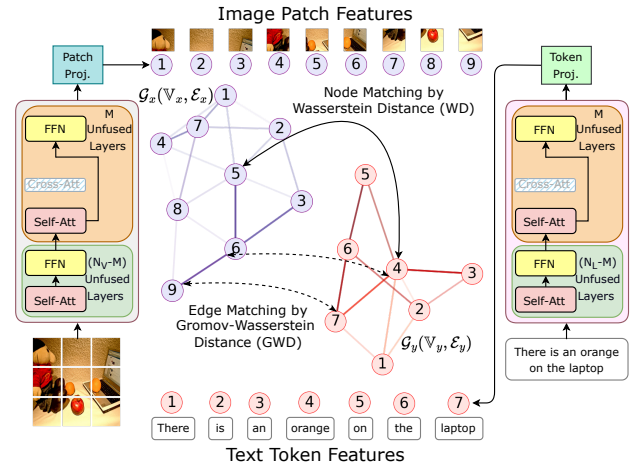


Figure 3: **Illustration of the graph optimal transport (GOT) algorithm used for patch-word alignment in the proposed VoLTA framework.** We obtain patch- and token-level features from the last layers of corresponding visual and textual transformer encoders and use these encoded local-feature vectors to construct modality-specific dynamic graphs - $\mathcal{G}_x(\mathbb{V}_x, \mathcal{E}_x)$ for image patches and $\mathcal{G}_y(\mathbb{V}_y, \mathcal{E}_y)$ for text tokens. Next, we perform patch-word alignment by utilizing the Gromov-Wasserstein distance and Wasserstein distance for edge and node matching, which preserves the topological graph structure. See Section 3.2 for details. Darker edges denote larger weights.

node in these graphs $i \in \{\mathbb{V}_x, \mathbb{V}_y\}$ is represented by corresponding feature vectors, and intermediate edges $e \in \{\mathbb{E}_x, \mathbb{E}_y\}$ by thresholded cosine similarity.

Importance of GOT in Patch-Word Alignment: As mentioned previously, GOT adopts two types of OT distances - WD for node matching and GWD for edge matching. In contrast, previous vision-language pre-training algorithms using OT for patch-word alignment only considered WD (Chen et al., 2020d; Kim et al., 2021). However, we argue that intricate images with multiple objects with similar shapes and colors require both WD and GWD for accurate, fine-grained matching. For example, in Figure 3, there are multiple “orange” present in the image. WD can only match nodes in the graph, and will treat all “orange” entities as identical and will ignore neighboring relations like “on the laptop”. However, by using proper edge matching with GWD, we can preserve the graph’s topological structure. We can correctly identify which “orange” in the image the sentence is referring to. Hence, we couple WD and GWD mutually beneficially and use a joint transport plan for accurate patch-word matching.

Once \mathcal{G}_x and \mathcal{G}_y are computed, we follow Chen et al. (2020a) to compute WD and GWD.

Wasserstein Distance calculates the pairwise distances between two sets of cross-domain node embeddings. Consider two discrete distributions, $\phi \in \mathbf{P}(\mathbb{X})$ and $\psi \in \mathbf{P}(\mathbb{Y})$, where $\phi = \sum_{i=1}^n u_i \delta_{x_i}$ and $\psi = \sum_{j=1}^m v_j \delta_{y_j}$; and δ_x being the Delta-Dirac function centered on x . Since ϕ and ψ are both probability distributions, sum of weight vectors is 1, $\sum_i u_i = 1 = \sum_j v_j$. The WD distance between ϕ and ψ is defined as:

$$\mathcal{D}_w(\phi, \psi) = \min_{\mathbf{T} \in \Pi(u, v)} \sum_i \sum_j \mathbf{T}_{ij} \cdot c(x_i, y_j) \quad (4)$$

where $\Pi(u, v) = \{\mathbf{T} \in \mathbb{R}_+^{n \times m} | \mathbf{T} \mathbf{1}_m = u, \mathbf{T}^\top \mathbf{1}_n = v\}$, $c(x_i, y_j)$ is cosine distance metric, and \mathbf{T} is the transport plan, interpreting the amount of mass shifted from ϕ_i to ψ_j .

Gromov-Wasserstein Distance assists in edge matching and preserves graph topology by calculating distances between pairs of nodes in each domain and measuring how these distances compare to the counter domain. In the same discrete graph matching setting, GWD between ϕ and ψ can be mathematically represented as:

$$\mathcal{D}_{gw}(\phi, \psi) = \min_{\hat{\mathbf{T}} \in \Pi(u, v)} \sum_{i, i', j, j'} \hat{\mathbf{T}}_{ij} \hat{\mathbf{T}}_{i'j'} L(x_i, y_j, x'_i, y'_j) \quad (5)$$

where intra-graph structural similarity between two node pairs (x_i, x'_i) and (y_j, y'_j) is represented as $L(x_i, y_j, x'_i, y'_j) = \|c_1(x_i, x'_i) - c_2(y_j, y'_j)\|$, c_i being cosine similarity between a node pair in any graph \mathcal{G}_i . Transport plan $\hat{\mathbf{T}}$ is periodically updated to align the edges in different graphs belonging to disparate modalities.

We further follow Chen et al. (2020a) to combine WD and GWD transport plans, leading to a unified GOT objective given as:

$$\mathcal{L}_{GOT}(\phi, \psi) = \gamma \mathcal{D}_w(\phi, \psi) + (1 - \gamma) \mathcal{D}_{gw}(\phi, \psi) \quad (6)$$

where γ regulates the importance of two loss terms.

3.3 Cross-Modal Attention Fusion (CMAF)

BT and GOT losses are computed in a dual encoder setting, which does not contain cross-modal interactions and is not suitable for complex multi-modal feature representation. Most existing methods, including UNITER (Chen et al., 2020d), ViLT (Kim et al., 2021), METER (Dou et al., 2022b), and GLIP (Li et al., 2022c) design cross-modal fusion by stacking additional transformer layers on top of uni-modal encoders, introducing a large number of added parameters during pre-training. We follow a more efficient solution proposed by FIBER (Dou et al., 2022a), which inserts cross-modal fusion into the uni-modal backbones with a gating mechanism. Specifically, at the top M transformer layers in the vision and language backbone,

cross-attention signals, weighted by a gating scalar α , are added to self-attention:

$$\begin{aligned}\hat{x} &= \text{Self-Att}(x) \\ x &= x + \hat{x} + \alpha * \text{Cross-Att}(\hat{x}, y) \\ x &= x + \text{FFN}(x)\end{aligned}\tag{7}$$

where α is a trainable parameter initialized to 0. Following existing literature (Li et al., 2021a; Wang et al., 2021a; Dou et al., 2022b;a), we use masked language modeling (MLM) and image-text matching (ITM) to pre-train the cross-attention parameters. For MLM, we randomly mask 15% text tokens, and the loss aims to reconstruct the masked tokens. We feed the network with randomly sampled image-caption pairs for ITM, and the loss predicts whether they are matched. The gating mechanism is a good choice for CMAF because (i) cross-attention parameters can easily be switched off by setting the gating scalar α to 0 when computing the BT and GOT losses. Thus, we can learn the cross-attention parameters without affecting the original computational flow of uni-modal backbones. (ii) gating mechanism is more lightweight and memory-efficient than adding fusion-specific layers (GLIP and METER use $4\times$ more fusion parameters than VoLTA).

Overall, VoLTA training pipeline can be summarized in the following three steps:

- **BT & GOT:** CMAF is switched off ($\alpha = 0$), VoLTA acts as dual encoder, \mathcal{L}_{BT} and \mathcal{L}_{GOT} are computed.
- **MLM & ITM:** CMAF is switched on ($\alpha \neq 0$), VoLTA now acts as fusion encoder, \mathcal{L}_{MLM} and \mathcal{L}_{ITM} losses are computed.
- **Back-propagation:** the four losses are added, giving $\mathcal{L}_{\text{total}} = \mathcal{L}_{\text{BT}} + w_{\text{GOT}} * \mathcal{L}_{\text{GOT}} + \mathcal{L}_{\text{MLM}} + \mathcal{L}_{\text{ITM}}$, and back-propagated into the model end-to-end. An ablation on different pre-training objectives of VoLTA and values of w_{GOT} is given in Section 4.7.

The overall VoLTA pipeline for computation of different training objectives is shown in Figure 2. The pseudo-code for VoLTA is presented in Appendix A.

3.4 Finetuning For Downstream Tasks

We adopt VoLTA to various vision- and vision-language downstream tasks. We switch off the inserted cross-attention modules for the vision-only tasks and use the image encoder. We utilize the learned cross-attention parameters as required for the vision-language tasks, following Dou et al. (2022a). For example, VQA and visual reasoning employ all cross-attention modules, whereas captioning requires only image-to-text cross-attention. Again, during IRTR, we switch off all cross-attentions and use VoLTA in a dual encoder setting. We keep all cross-attention parameters during multi-modal object detection and referring expression comprehension and train an object detection head from scratch using the language-aware image features.

4 Experiments, Results, and Analysis

4.1 Pre-training & Downstream datasets

Following Chen et al. (2020d) and Huang et al. (2021), we perform pre-training by appending the VG dataset (Krishna et al., 2017) with COCO2017 (Lin et al., 2014), together consisting of 231k images. We divide our downstream tasks into three categories - (i) **Uni-modal tasks** such as image classification on ImageNet (Deng et al., 2009), VOC07 (Everingham et al., 2010), COCO; object detection on VOC07+12, COCO, and instance segmentation on COCO. (ii) **Multi-modal fine-grained tasks** such as region-level VL tasks - referring expression comprehension (REC) on RefCOCO, RefCOCO+, RefCOCOg (Kazemzadeh et al., 2014; Yu et al., 2016), and language-conditioned object detection on COCO and LVIS (Gupta et al., 2019). (iii) **Multi-modal coarse-grained tasks** such as image-level VL tasks - visual question answering on VQAv2 (Antol et al., 2015), visual reasoning on NLVR² (Suhr et al., 2019), image- and text retrieval on Flickr30k (Plummer et al., 2015) and captioning on COCO. We exclude any overlap between our pre-training and downstream validation/test splits. Detailed statistics of all downstream datasets are given in Appendix C.

Linear probing on ImageNet Validation Set					Linear probing on VOC07 and COCO						
Method	Pre-train	Arch.	Pre-training Supervision	Top-1	Method	Pre-train	Arch.	VOC07		COCO	
								SVM	MLP	MLP (PC/O)	MLP (PC/O)
Sup.	IN-1K	RN50	Label	76.5	Sup.	IN-1K	RN50	87.5	90.8	55.2/60.8	
Sup.	IN-100	RN50	Label	53.3 [†]	BYOL	IN-1K	RN50	86.6	—	—	
MoCo	COCO	RN50	NA	44.5 [†]	BT	IN-1K	RN50	86.2	91.9 [‡]	56.1/63.0 [‡]	
MoCo-v2	COCO	RN50	NA	49.3 [‡]	VICReg	IN-1K	RN50	86.6	91.1 [‡]	51.0/57.9 [‡]	
CAST	COCO	RN50	Caption	48.7	CAST	COCO	RN50	74.0	—	51.0/57.9	
VirTex	COCO	RN50	Caption	52.8	VirTex	COCO	RN50	88.7	—	—	
ICMLM	COCO	RN50	Caption	51.9	ICMLM	COCO	RN50	87.5	—	—	
MCT	COCO	RN50	Caption	54.9	LocTex	COCO	RN50	88.4	—	—	
MCT	COCO	RN50	Caption+Tag	55.3	LocTex	COCO+OpenIm	RN50	92.6	—	—	
VoLTA(w/o MLM, ITM)	COCO	RN50	Caption	55.3	VoLTA(w/o MLM, ITM)	COCO	RN50	89.6	94.3	71.4/74.3	
VoLTA(w/o MLM, ITM)	COCO	Swin-T	Caption	56.3	VoLTA(w/o MLM, ITM)	COCO	Swin-T	88.2	93.5	73.4/75.7	
VoLTA(w/o MLM, ITM)	COCO	Swin-B	Caption	62.5	VoLTA(w/o MLM, ITM)	COCO	Swin-B	88.5	93.9	74.1/76.1	
VoLTA	COCO	Swin-B	Caption	62.5	VoLTA	COCO	Swin-B	89.7	95.0	74.5/76.4	

Table 1: **Uni-modal downstream: linear image classification.** We benchmark learned representations on image classification tasks by training linear classifiers on fixed features. We report top-1 accuracy on ImageNet-1k validation set, classification mAP on VOC07, and per-class (PC) and overall (O) F1 scores on COCO. Numbers with [†] are re-implemented by Yuan et al. (2021), and the numbers with [‡] are re-implemented by us. methods trained with significantly larger datasets are colored gray. The best results are in **bold**.

Method	Pre-train	Arch.	Pre-training Supervision	VOC07+12 det			COCO det			COCO instance seg		
				AP _{all}	AP ₅₀	AP ₇₅	AP ^{bb}	AP ₅₀ ^{bb}	AP ₇₅ ^{bb}	AP ^{mk}	AP ₅₀ ^{mk}	AP ₇₅ ^{mk}
Sup.	IN-1K	RN50	Label	53.5	81.3	58.8	38.2	58.2	41.2	33.3	54.7	35.2
MoCo-v2 [†]	IN-1K	RN50	NA	57.4	82.5	64.0	39.3	58.9	42.5	34.4	55.8	36.5
MoCo	COCO	RN50	NA	47.5	75.4	51.1	38.5	58.5	42.0	35.0	55.6	37.5
MoCo-v2	COCO	RN50	NA	48.4	75.5	52.1	39.8	59.6	43.1	35.8	56.9	38.8
CAST	COCO	RN50	Caption	54.2	80.1	59.9	39.4	60.0	42.8	35.8	57.1	38.6
VirTex	COCO	RN50	Caption	55.6	81.4	61.5	40.9	61.7	44.8	36.9	58.4	39.7
LocTex	COCO	RN50	Caption	53.9	80.9	59.8	40.6	60.6	44.1	35.2	57.0	37.4
MCT	COCO	RN50	Caption	56.1	82.1	62.4	41.1	61.8	44.9	36.9	58.2	40.0
VoLTA	COCO	RN50	Caption	56.6	84.4	62.7	41.9	61.8	44.8	36.5	58.5	40.8
Sup. [‡]	IN-1K	Swin-T	Label	—	—	—	50.5	69.3	54.9	43.7	66.6	47.1
MoBY [‡]	IN-1K	Swin-T	NA	—	—	—	50.2	68.8	54.7	43.5	66.1	46.9
VoLTA	COCO	Swin-T	Caption	—	—	—	50.9	69.6	55.5	43.8	66.9	47.5
Sup. [‡]	IN-1K	Swin-B	Label	—	—	—	51.9	70.9	56.5	45.0	68.4	48.7
ViTDet	IN-1K	ViT-B	NA	—	—	—	51.6	—	—	45.9	—	—
CLIP	LAION-20M	ViT-B	Caption	—	—	—	45.2	—	—	40.4	—	—
SLIP	LAION-20M	ViT-B	Caption	—	—	—	44.7	—	—	41.0	—	—
MaskCLIP	LAION-20M	ViT-B	Caption	—	—	—	46.6	—	—	41.7	—	—
VoLTA	COCO	Swin-B	Caption	—	—	—	52.1	71.3	56.6	45.2	68.5	49.0

Table 2: **Uni-modal downstream: object detection and instance segmentation with fine-tuning.** We benchmark learned representations on VOC07+12 object detection task using faster R-CNN (Ren et al., 2015), and on COCO2017 object detection and instance segmentation using mask R-CNN (He et al., 2017), both with C4 backbone variant (Wu et al., 2019). The best results are in **bold**. Methods marked with [†] and [‡] are not direct comparison to other baselines as they use multiple MLP layers & significant data augmentations and cascade mask R-CNN (Cai & Vasconcelos, 2018) during fine-tuning, respectively.

4.2 Network Architectures

Following FIBER (Dou et al., 2022a), we adopt Swin-Base (Liu et al., 2021) and RoBERTa-Base (Liu et al., 2019) as our vision and text encoders, which are initialized with weights from uni-modal pre-training. We collect patch- and token features from the last transformer layers, feed them into the local projector network, and compute GOT loss. Furthermore, we apply AvgPool on patch and token features, feed them into the global projector network, and compute BT loss. Both local and global projector networks have three linear layers with dimensions 2048-2048-1024, with batch normalization and ReLU after the first two layers. Section 4.7 gives an ablation on projector dimension. We use the image and text features after the AvgPool layer during downstream tasks. For CMAF, we insert the cross-attention into the top 6 blocks of the vision and text encoders. Moreover, for direct comparison with existing uni-modal baselines, we re-train VoLTA with ResNet50 (He et al., 2016) and Swin-Tiny image encoders.

Method	#Pre-train Data		RefCOCO			RefCOCO+			RefCOCOg	
	I-T	I-T-B	val	testA	testB	val	testA	testB	val	test
MAttNet	—	—	76.4	80.4	69.3	64.9	70.3	56.0	66.7	67.0
VLBERT	3M	—	—	—	—	71.6	77.7	61.0	—	—
ViLBERT	3M	—	—	—	—	72.3	78.5	62.6	—	—
Ernie-VL-L	4M	—	—	—	—	75.9	82.4	66.9	—	—
Rosita	4M	—	84.8	88.0	78.3	76.1	82.0	67.4	78.2	78.3
UNITER-L	4M	—	81.4	87.0	74.2	75.9	81.5	66.7	74.9	75.8
VILLA-L	4M	—	82.4	87.5	74.8	76.2	81.5	66.9	76.2	76.7
<i>Models pre-trained on Im-Txt-Box data</i>										
MDETR-B	—	1.3M	87.5	90.4	82.7	81.1	85.5	73.0	83.4	83.3
UniTAB	—	1.3M	86.3	88.8	80.6	78.7	83.2	69.5	80.0	80.0
X-VLM	4M	6.15M	—	—	—	80.2	86.4	71.0	—	—
OFA-L	16M	3M	90.1	92.9	85.3	84.5	90.1	77.8	84.5	85.2
FIBER-B	4M	0.8M	90.7	92.6	87.3	85.7	90.1	79.4	87.1	87.3
VoLTA-B	231k	—	86.1	88.6	81.8	77.0	82.7	67.8	78.3	78.3

Table 3: **Multi-modal fine-grained downstream: referring expression comprehension.** Methods pre-trained on image-text-box (I-T-B) data are colored gray. Best comparable results are in **bold**. VoLTA-B denotes Swin-B backbone.

Method	COCO Val 2017		LVIS MiniVal			
	AP	APr	APc	APf	AP	
<i>Models pre-trained on Im-Txt-Box and/or with larger size</i>						
Mask R-CNN	—	—	26.3	34.0	33.9	33.3
MDETR	—	—	20.9	24.9	24.3	24.2
GLIP-B	57.0	—	31.3	48.3	56.9	51.0
GLIP-L	60.8	—	—	—	—	—
FIBER-B	58.4	—	50.0	56.9	58.1	56.9
VoLTA-B	51.6	34.4	43.1	43.8	42.7	

Table 4: **Multi-modal fine-grained downstream: language-conditioned object detection on COCO and LVIS.** All available baselines are pre-trained on Im-Txt-Box data and are colored gray. VoLTA-B denotes Swin-B backbone.

4.3 Implementation Details

We perform pre-training for 20 epochs with 256 batch-size on 64 V100 GPUs. Following [Zbontar et al. \(2021\)](#), we use the LARS optimizer ([You et al., 2017](#)) with a learning rate of 0.2 for the weights and 0.0048 for the biases and batch normalization parameters. We use a learning rate warm-up period of 2 epochs, after which we reduce the learning rate by a factor of 1000 using a cosine decay schedule ([Loshchilov & Hutter, 2016](#)). We use $1e-6$ weight decay, excluding the biases and batch normalization parameters. We conduct a grid search for the GOT loss hyperparameter (w_{GOT}), and we empirically found the best value to be 100. Appendix D explains other necessary pre-training and downstream hyper-parameters details.

4.4 Results on Vision-only tasks

We first experiment on three uni-modal tasks - classification, object detection, and instance segmentation. For a direct comparison with existing ResNet50 and Swin-T baselines, we re-train identical encoders with VoLTA pipeline. Furthermore, since the uni-modal tasks do not utilize cross-attention parameters, we perform an ablation by dropping the MLM and ITM objectives from VoLTA.

Image Classification: Table 1 presents the linear probing results of uni-label classification on ImageNet and multi-label classification on VOC07 and COCO. For all uni-modal tasks, we report results with COCO pre-training for a fair comparison with existing baselines. For ImageNet, we adopt all COCO baselines from [Yuan et al. \(2021\)](#). Even without the MLM and ITM objectives, VoLTA achieves better performance than all baselines across three datasets with ResNet50 backbone. The Swin backbones and cross-attention module further improve the performance. For VOC07, we report the results for both SVM and MLP-based linear classifiers. VoLTA with ResNet50 backbone achieves state-of-the-art results on VOC07 SVM evaluation, beating the nearest baseline, SwAV, by 0.7 mAP score. These results indicate the ability of VoLTA to learn effective image-level visual features.

Method	#Pre-train Data	VQAv2		NLVR ²		F30k IRTR		Method	#Pre-train Data	COCO Captioning			
		dev	std	dev	test-P	IR@1	TR@1			B@4	M	C	S
<i>Models pre-trained on COCO (123k) and/or VG (108k)</i>													
SCAN	108k	—	—	—	—	48.6	67.4	ViTEx	123k	—	—	95.5	18.1
SCG	108k	—	—	—	—	49.3	71.8	VL-T5	180k	34.5	28.7	116.5	21.9
PFAN	108k	—	—	—	—	50.4	70.0	VL-BART	180k	35.1	28.7	116.6	21.5
MaxEnt	123k	54.1	54.8	—	—	—	—	VLTA-B	231k	38.2	30.7	126.6	22.5
VisualBERT	123k	70.8	71.0	67.4	67.0	—	—	VLTA-GOLD-B	231k	38.9	30.5	128.5	23.4
LXMERT	231k	72.4	72.5	74.9	74.5	—	—	<i>Models fine-tuned without CIDEr optimization</i>					
SOHO	231k	73.2	73.4	76.3	77.3	72.5	86.5	VLTA-B	231k	39.7	30.5	133.6	23.7
VLTA-B	231k	74.6	74.6	76.7	78.1	72.7	83.6	VLTA-GOLD-B	231k	40.2	30.9	137.5	23.7

Table 5: **Multi-modal coarse-grained downstream: visual question answering, visual reasoning, retrieval, and captioning.** We only compare with methods pre-trained on a comparable amount of dataset. For captioning, 4 metrics are reported - B@4: BLEU@4, M: METEOR, C: CIDEr, S: SPICE. The best results are in **bold**. VLTA-B denotes Swin-B backbone.

\mathcal{L}_{BT}	VoLTA				RefCOCO			RefCOCO+			RefCOCOg	
	\mathcal{L}_{GOT}		\mathcal{L}_{MLM}	\mathcal{L}_{ITM}	val	testA	testB	val	testA	testB	val	test
	\mathcal{L}_{w}	\mathcal{L}_{gw}										
✓	—	—	—	—	81.7	84.1	77.8	71.2	76.6	62.2	71.7	71.7
—	—	—	✓	✓	82.0	84.5	77.8	71.5	77.1	62.2	71.4	71.8
✓	—	—	✓	✓	82.7	85.2	78.1	72.0	77.7	62.5	72.8	72.7
✓	✓	—	✓	✓	83.9	86.6	80.5	73.9	79.5	64.1	74.6	74.3
✓	—	✓	✓	✓	82.8	85.5	78.5	72.2	77.8	62.8	72.9	72.8
✓	✓	✓	✓	✓	86.1	88.6	81.8	77.0	82.7	67.8	78.3	78.3

Table 6: **Ablation study on different losses of the training objective of VoLTA for referring expression comprehension tasks.** Each model is pre-trained on 231k samples from COCO2017 and VG.

Object Detection & Instance Segmentation: Next, we perform two uni-modal region-level tasks - object detection on VOC07 + 12 and COCO2017, and instance segmentation on COCO2017. As shown in Table 2, VoLTA yields the state-of-the-art performance in both tasks across the majority of metrics. The fine-grained region-level understanding helps VoLTA to perform well on detection and segmentation tasks.

4.5 Results on Fine-grained Vision-Language tasks

Next, we perform region-level multi-modal downstream tasks - referring expression comprehension (REC) and language-guided object detection.

REC: This task aims to localize target objects in an image described by a referring expression phrased in natural language and, thus, perfectly evaluates the fine-grained feature representation capability of VoLTA. As depicted in Table 3, VoLTA beats larger-sized UNITER-L and VILLA-L models on the challenging testB split of both RefCOCO and RefCOCO+. Moreover, VoLTA performs comparably with MDETR and UniTAB, even without being trained on grounding data. These results indicate our model’s efficacy in learning fine-grained local visual features.

Object Detection: We evaluate VoLTA on two challenging language-conditioned object detection benchmarks - COCO and LVIS. Note that, all existing baselines for this tasks are pre-trained on fine-grained *image-text-box* data, whereas VoLTA only utilizes *image-caption* pairs. Table 4 shows that VoLTA performs comparatively with these strong baselines. Note that VoLTA beats Mask R-CNN, MDETR, and GLIP-B on LVIS APr, which denotes average precision on rare objects. Thus, we conclude that VoLTA achieves impressive localization ability and robustness, even without utilizing any grounding annotations.

4.6 Results on Coarse-grained Vision-Language tasks

Next, we perform image-level multi-modal downstream tasks - visual question answering (VQA), visual reasoning, retrieval, and captioning.

VQA & Visual Reasoning: As reported in Table 5, VoLTA achieves the best performance on VQA and visual reasoning across the baselines pre-trained with a comparable amount of data. Moreover, on VQA,

				VOC07	COCO		VOC07	COCO		VOC07	COCO
				MLP	MLP (PC/O)		MLP	MLP (PC/O)		MLP	MLP (PC/O)
✓	—	—	—	90.8	72.2/71.7		50	93.4	74.1/76.0	8192-8192-128	91.3
✓	✓	—	—	91.8	74.0/73.7		100	94.0	74.5/76.4	8192-8192-256	91.9
—	—	✓	✓	86.5	69.0/69.8		200	93.2	73.1/75.5	2048-2048-512	93.4
✓	✓	✓	✓	94.0	74.5/76.4		500	93.1	72.8/75.3	2048-2048-1024	94.0

(a) **Ablation study on Intra- and Inter-modal Barlow Twins objective** for multi-label image classification on VOC07 and COCO.

(b) **Ablation study on the value of w_{GOT}** , the weight of GOT loss in $\mathcal{L}_{\text{total}}$ in the objective of VoLTA for multi-label image classification on VOC07 and COCO.

Projector Config.	VOC07	COCO
	MLP	MLP (PC/O)
8192-8192-128	91.3	71.3/73.0
8192-8192-256	91.9	72.2/73.3
2048-2048-512	93.4	73.9/76.1
2048-2048-1024	94.0	74.5/76.4

(c) **Ablation study on the dimension of local and global projector networks** of VoLTA for multi-label image classification on VOC07 and COCO.

Table 7: **Ablation on Intra- and Inter-modal Barlow Twins objective (a), the value of w_{GOT} (b), and the dimension of projector networks (c)**. We report classification mAP on VOC07, and per-class (PC) and overall (O) F1 scores on COCO. Each model is pre-trained on 123k train-val samples from COCO2017.

VoLTA beats LXMERT, which is trained with $2\times$ more data. These results demonstrate the efficacy of our method even when utilizing a mid-scale pre-training corpus.

Retrieval: Most existing VLP methods use a fusion encoder for image and text retrieval and feed every image-text pair into the model. Though such fine-tuning often results in higher performance, it introduces quadratic time cost and is not scalable. Following Dou et al. (2022a), we adopt a more efficient strategy. We drop the cross-attention parameters for this task and compute the dot product of image and text features extracted separately in the dual-encoder setting. As shown in Table 5, even with such an approach, VoLTA produces superior performance among the baselines trained with a similar amount of data, beating all three baselines by a significant margin.

Captioning: We perform captioning on the COCO dataset to evaluate if VoLTA can adopt a generation task. We integrate GOLD (Pang & He, 2021) into VoLTA during fine-tuning as it produces significant improvements. As shown in Table 5, our approach maintains superior captioning performance across all baselines pre-trained with comparable data. Using CIDEr optimization further improves performance.

It is worth mentioning that besides achieving a superior result than all baselines using a comparable amount of data on multi-modal coarse-grained tasks, VoLTA also outperforms multiple methods pre-trained using magnitude more data. These results, shown in Table F.1, indicate the effectiveness and generalizability of VoLTA across these tasks.

4.7 Ablation Study

We perform ablation studies on the pre-training objectives, GOT loss weight, and the dimension of projectors.

Pre-training Objectives: We ablate the effectiveness of different pre-training objectives and evaluate the pre-trained models on fine-grained downstream tasks. First, we pre-train VoLTA only with the multi-modal BT loss. In this setup, VoLTA only acts as a dual encoder; thus, the cross-attention parameters are not pre-trained. Next, we add MLM and ITM loss which helps the model to learn cross-modal information via attention fusion. Next, we add the GOT pre-training objective. Note that GOT adopts two types of OT distances – WD for node matching and GWD for edge matching. As shown in table 6, applying WD and GWD together improves the performance of reference expression comprehension across RefCOCO, RefCOCO+, and RefCOCOg datasets. Specifically on RefCOCOg, adding \mathcal{L}_{gw} to \mathcal{L}_{w} yields a significant 4.0% boost in the challenging test set. Since this dataset contains intricate images with multiple similar objects with different shapes and colors, GWD is crucial in distinguishing between them. However, we see that adding GWD without WD is not helpful. This is because though GWD can capture the edge similarity between graphs, it cannot directly address graph alignment since it does not consider node information. For example, the word pair (boy, girl) has a similar cosine similarity as the pair (football, basketball). Still, the semantic meanings of the two pairs are different and should not be matched. But GWD will treat these two



Figure 4: **Visualization of fine-grained patch-word alignment, produced by VoLTA.** We look at the optimal transport plan from GOT to represent the alignment between the words in red with the corresponding input image. All image-caption pairs are taken from the COCO2017 train split. The visualizations are generated with 224p images, resulting in sequences of 196 tokens for 16×16 patches.

pairs as the same since it only considers the cosine similarity between nodes. Hence, when applied together, WD and GWD objectives only result in an effective region-word alignment.

We also verify the effectiveness of the multi-modal BT objective by ablating the intra- and inter-modal terms. The first row of Table 7a is identical to the original image-only BT objective. Next, we introduce the text branch and add the same BT objective between the two views of the caption. Afterward, we add the inter-modal BT objectives. As shown in Table 7a, each loss term improved the image classification performance, demonstrating the importance of intra- and inter-modal objectives. Overall, this set of experiments demonstrates that all objectives are necessary for our model to perform well on different fine-grained multi-modal tasks.

GOT Loss Weight: In our loss formulation, we introduce a GOT loss weight w_{GOT} which regulates the alignment of local features through GOT loss. By conducting a grid search on uni-modal downstream classification tasks, we assessed the impact of w_{GOT} as shown in Table 7b and experimentally found its best value to be 100 in our case. It is to be noted that a very high value of w_{GOT} considerably degrades the performance of downstream tasks.

Ablation on Projector Dimension: The design of the projector head plays a pivotal role in the downstream performance of the model (Garrido et al., 2022). To investigate the impact of hidden and feature (projector output) dimensions, we have tested 4 different configurations on uni-modal downstream classification tasks. It can be observed (see Table 7c) that an increase in the number of parameters in the projector head does not necessarily lead to an increase in performance. For example, a projector configuration of 8192-8192-256 has roughly eight times more parameters than 2048-2048-1024. However, the latter performs better in downstream tasks (Table 7c), indicating that the output dimension of the projector plays a crucial role in the final performance of the model.

4.8 Qualitative Results & Error Analysis

Figure 4 shows the fine-grained alignment of image regions and caption words achieved by the pre-trained VolTA system. The transport plan from GOT module outputs the similarity across every image patch and caption token. To obtain the visualizations in Figure 4, we choose the similarity scores between the red words in the caption with every image patch. Next, we apply bilinear interpolation to these similarity scores to convert them to the same dimension as the input image. Finally, we superimpose these interpolated similarity maps on the input images to obtain Figure 4 as the outcome. In most cases, the pre-trained model accurately learns to localize various objects using only global image-caption data. However, objects in extremely cluttered scenarios are occasionally not focused. We show such error cases in Section E.

5 Conclusion

We present VoLTA, a unified VLP paradigm that utilizes image-caption data but achieves fine-grained region-level image understanding, eliminating the use of expensive box annotations. VoLTA adopts graph optimal transport-based weakly supervised patch-token alignment and produces an explicit, self-normalized, and interpretable low-level matching criterion. Extensive experiments demonstrate the effectiveness of VoLTA on a wide range of coarse- and fine-grained tasks.

Acknowledgement

The codebase for this work is built on the Barlow Twins (Zbontar et al., 2021), GOT (Chen et al., 2020a), and FIBER (Dou et al., 2022a) repository. We would like to thank the respective authors for their contribution, and the Meta AI team for discussions and feedback. Shraman Pramanick and Rama Chellappa were partially supported by an ONR MURI Grant N00014-20-1-2787.

References

Peter Anderson, Basura Fernando, Mark Johnson, and Stephen Gould. Spice: Semantic propositional image caption evaluation. In *European Conference on Computer Vision*, pp. 382–398. Springer, 2016.

Stanislaw Antol, Aishwarya Agrawal, Jiasen Lu, Margaret Mitchell, Dhruv Batra, C Lawrence Zitnick, and Devi Parikh. Vqa: Visual question answering. In *International Conference on Computer Vision*, pp. 2425–2433, 2015.

Mahmoud Assran, Mathilde Caron, Ishan Misra, Piotr Bojanowski, Florian Bordes, Pascal Vincent, Armand Joulin, Michael G. Rabbat, and Nicolas Ballas. Masked siamese networks for label-efficient learning. *arXiv*, abs/2204.07141, 2022.

Yogesh Balaji, Rama Chellappa, and Soheil Feizi. Normalized wasserstein for mixture distributions with applications in adversarial learning and domain adaptation. In *International Conference on Computer Vision*, pp. 6500–6508, 2019.

Satanjeev Banerjee and Alon Lavie. Meteor: An automatic metric for mt evaluation with improved correlation with human judgments. In *Proceedings of the ACL Workshop on Intrinsic and Extrinsic Evaluation Measures for Machine Translation and/or Summarization*, pp. 65–72, 2005.

Hangbo Bao, Li Dong, Songhao Piao, and Furu Wei. Beit: Bert pre-training of image transformers. In *International Conference on Learning Representations*, 2021.

Adrien Bardes, Jean Ponce, and Yann LeCun. Vicreg: Variance-invariance-covariance regularization for self-supervised learning. In *International Conference on Learning Representations*, 2022.

Tom Brown, Benjamin Mann, Nick Ryder, Melanie Subbiah, Jared D Kaplan, Prafulla Dhariwal, Arvind Neelakantan, Pranav Shyam, Girish Sastry, Amanda Askell, et al. Language models are few-shot learners. *Advances in Neural Information Processing Systems*, 33:1877–1901, 2020.

Zhaowei Cai and Nuno Vasconcelos. Cascade r-cnn: Delving into high quality object detection. In *Proceedings of the IEEE/CVF Conference on Computer Vision and Pattern Recognition*, pp. 6154–6162, 2018.

Mathilde Caron, Hugo Touvron, Ishan Misra, Herv'e J'egou, Julien Mairal, Piotr Bojanowski, and Armand Joulin. Emerging properties in self-supervised vision transformers. *International Conference on Computer Vision*, pp. 9630–9640, 2021.

Chun-Fu (Richard) Chen, Quanfu Fan, and Rameswar Panda. CrossViT: Cross-Attention Multi-Scale Vision Transformer for Image Classification. In *International Conference on Computer Vision*, 2021a.

Liqun Chen, Yizhe Zhang, Ruiyi Zhang, Chenyang Tao, Zhe Gan, Haichao Zhang, Bai Li, Dinghan Shen, Changyou Chen, and Lawrence Carin. Improving sequence-to-sequence learning via optimal transport. In International Conference on Learning Representations, 2019. URL <https://openreview.net/forum?id=S1xtAjR5tX>.

Liqun Chen, Zhe Gan, Yu Cheng, Linjie Li, Lawrence Carin, and Jingjing Liu. Graph optimal transport for cross-domain alignment. In International Conference on Machine Learning, pp. 1542–1553. PMLR, 2020a.

Ting Chen, Simon Kornblith, Mohammad Norouzi, and Geoffrey Hinton. A simple framework for contrastive learning of visual representations. In International Conference on Machine Learning, pp. 1597–1607. PMLR, 2020b.

Xinlei Chen and Kaiming He. Exploring simple siamese representation learning. Proceedings of the IEEE/CVF Conference on Computer Vision and Pattern Recognition, pp. 15745–15753, 2021.

Xinlei Chen, Haoqi Fan, Ross Girshick, and Kaiming He. Improved baselines with momentum contrastive learning. arXiv preprint arXiv:2003.04297, 2020c.

Xinlei Chen, Saining Xie, and Kaiming He. An empirical study of training self-supervised vision transformers. International Conference on Computer Vision, pp. 9620–9629, 2021b.

Yen-Chun Chen, Linjie Li, Licheng Yu, Ahmed El Kholy, Faisal Ahmed, Zhe Gan, Yu Cheng, and Jingjing Liu. Uniter: Universal image-text representation learning. In European Conference on Computer Vision, pp. 104–120. Springer, 2020d.

Jaemin Cho, Jie Lei, Hao Tan, and Mohit Bansal. Unifying vision-and-language tasks via text generation. In International Conference on Machine Learning, pp. 1931–1942. PMLR, 2021.

Xiyang Dai, Yinpeng Chen, Bin Xiao, Dongdong Chen, Mengchen Liu, Lu Yuan, and Lei Zhang. Dynamic head: Unifying object detection heads with attentions. In Proceedings of the IEEE/CVF Conference on Computer Vision and Pattern Recognition, pp. 7373–7382, 2021.

Jia Deng, Wei Dong, Richard Socher, Li-Jia Li, Kai Li, and Li Fei-Fei. Imagenet: A large-scale hierarchical image database. In Proceedings of the IEEE Conference on Computer Vision and Pattern Recognition, pp. 248–255. Ieee, 2009.

Jacob Devlin, Ming-Wei Chang, Kenton Lee, and Kristina Toutanova. Bert: Pre-training of deep bidirectional transformers for language understanding. In Proceedings of the 2019 Conference of the North American Chapter of the Association for Computational Linguistics: Human Language Technologies, Volume 1 (Long and Short Papers), pp. 4171–4186, 2019.

Alexey Dosovitskiy, Lucas Beyer, Alexander Kolesnikov, Dirk Weissenborn, Xiaohua Zhai, Thomas Unterthiner, Mostafa Dehghani, Matthias Minderer, Georg Heigold, Sylvain Gelly, Jakob Uszkoreit, and Neil Houlsby. An image is worth 16x16 words: Transformers for image recognition at scale. In International Conference on Learning Representations, 2021. URL <https://openreview.net/forum?id=YicbFdNTTy>.

Zi-Yi Dou, Aishwarya Kamath, Zhe Gan, Pengchuan Zhang, Jianfeng Wang, Linjie Li, Zicheng Liu, Ce Liu, Yann LeCun, Nanyun Peng, et al. Coarse-to-fine vision-language pre-training with fusion in the backbone. Advances in Neural Information Processing Systems, 2022a.

Zi-Yi Dou, Yichong Xu, Zhe Gan, Jianfeng Wang, Shuohang Wang, Lijuan Wang, Chenguang Zhu, Pengchuan Zhang, Lu Yuan, Nanyun Peng, et al. An empirical study of training end-to-end vision-and-language transformers. In Proceedings of the IEEE/CVF Conference on Computer Vision and Pattern Recognition, pp. 18166–18176, 2022b.

Mark Everingham, Luc Van Gool, Christopher KI Williams, John Winn, and Andrew Zisserman. The pascal visual object classes (voc) challenge. International Journal of Computer Vision, 88(2):303–338, 2010.

Tianyu Gao, Xingcheng Yao, and Danqi Chen. Simcse: Simple contrastive learning of sentence embeddings. In Proceedings of the 2021 Conference on Empirical Methods in Natural Language Processing, pp. 6894–6910, 2021.

Quentin Garrido, Yubei Chen, Adrien Bardes, Laurent Najman, and Yann Lecun. On the duality between contrastive and non-contrastive self-supervised learning. arXiv preprint arXiv:2206.02574, 2022.

Aude Genevay, Gabriel Peyré, and Marco Cuturi. Learning generative models with sinkhorn divergences. In International Conference on Artificial Intelligence and Statistics, pp. 1608–1617. PMLR, 2018.

Xinyang Geng, Hao Liu, Lisa Lee, Dale Schuurmans, Sergey Levine, and P. Abbeel. Multimodal masked autoencoders learn transferable representations. arXiv, abs/2205.14204, 2022.

Priya Goyal, Piotr Dollár, Ross Girshick, Pieter Noordhuis, Lukasz Wesolowski, Aapo Kyrola, Andrew Tulloch, Yangqing Jia, and Kaiming He. Accurate, large minibatch sgd: Training imagenet in 1 hour. arXiv preprint arXiv:1706.02677, 2017.

Jean-Bastien Grill, Florian Strub, Florent Altché, Corentin Tallec, Pierre Richemond, Elena Buchatskaya, Carl Doersch, Bernardo Avila Pires, Zhaohan Guo, Mohammad Gheshlaghi Azar, et al. Bootstrap your own latent-a new approach to self-supervised learning. Advances in Neural Information Processing Systems, 33:21271–21284, 2020.

Agrim Gupta, Piotr Dollar, and Ross Girshick. Lvis: A dataset for large vocabulary instance segmentation. In Proceedings of the IEEE Conference on Computer Vision and Pattern Recognition, pp. 5356–5364, 2019.

Song Han, Jeff Pool, John Tran, and William Dally. Learning both weights and connections for efficient neural network. Advances in Neural Information Processing Systems, 28, 2015.

Xiao Han, Xiatian Zhu, Licheng Yu, Li Zhang, Yi-Zhe Song, and Tao Xiang. Fame-vil: Multi-tasking vision-language model for heterogeneous fashion tasks. In Proceedings of the IEEE/CVF Conference on Computer Vision and Pattern Recognition, pp. 2669–2680, 2023.

Kaiming He, Xiangyu Zhang, Shaoqing Ren, and Jian Sun. Deep residual learning for image recognition. In Proceedings of the IEEE Conference on Computer Vision and Pattern Recognition, pp. 770–778, 2016.

Kaiming He, Georgia Gkioxari, Piotr Dollár, and Ross Girshick. Mask r-cnn. In International Conference on Computer Vision, pp. 2961–2969, 2017.

Kaiming He, Haoqi Fan, Yuxin Wu, Saining Xie, and Ross Girshick. Momentum contrast for unsupervised visual representation learning. In Proceedings of the IEEE/CVF Conference on Computer Vision and Pattern Recognition, pp. 9729–9738, 2020.

Kaiming He, Xinlei Chen, Saining Xie, Yanghao Li, Piotr Dollár, and Ross Girshick. Masked autoencoders are scalable vision learners. In Proceedings of the IEEE/CVF Conference on Computer Vision and Pattern Recognition, pp. 16000–16009, 2022.

Zhicheng Huang, Zhaoyang Zeng, Bei Liu, Dongmei Fu, and Jianlong Fu. Pixel-bert: Aligning image pixels with text by deep multi-modal transformers. arXiv preprint arXiv:2004.00849, 2020.

Zhicheng Huang, Zhaoyang Zeng, Yupan Huang, Bei Liu, Dongmei Fu, and Jianlong Fu. Seeing out of the box: End-to-end pre-training for vision-language representation learning. In Proceedings of the IEEE/CVF Conference on Computer Vision and Pattern Recognition, pp. 12976–12985, 2021.

Jiho Jang, Chaerin Kong, Donghyeon Jeon, Seonhoon Kim, and Nojun Kwak. Unifying vision-language representation space with single-tower transformer. In Proceedings of the AAAI Conference on Artificial Intelligence, 2023.

Chao Jia, Yinfei Yang, Ye Xia, Yi-Ting Chen, Zarana Parekh, Hieu Pham, Quoc Le, Yun-Hsuan Sung, Zhen Li, and Tom Duerig. Scaling up visual and vision-language representation learning with noisy text supervision. In *International Conference on Machine Learning*, pp. 4904–4916. PMLR, 2021.

Aishwarya Kamath, Mannat Singh, Yann LeCun, Gabriel Synnaeve, Ishan Misra, and Nicolas Carion. Mdetr-modulated detection for end-to-end multi-modal understanding. In *International Conference on Computer Vision*, pp. 1780–1790, 2021.

Sahar Kazemzadeh, Vicente Ordonez, Mark Matten, and Tamara Berg. Referitgame: Referring to objects in photographs of natural scenes. In *Proceedings of the 2014 Conference on Empirical Methods in Natural Language Processing*, pp. 787–798, 2014.

Douwe Kiela, Suvrat Bhooshan, Hamed Firooz, and Davide Testuggine. Supervised multimodal bitransformers for classifying images and text. *arXiv*, abs/1909.02950, 2019.

Wonjae Kim, Bokyung Son, and Ildoo Kim. Vilt: Vision-and-language transformer without convolution or region supervision. In *International Conference on Machine Learning*, pp. 5583–5594. PMLR, 2021.

Ranjay Krishna, Yuke Zhu, Oliver Groth, Justin Johnson, Kenji Hata, Joshua Kravitz, Stephanie Chen, Yannis Kalantidis, Li-Jia Li, David A Shamma, et al. Visual genome: Connecting language and vision using crowdsourced dense image annotations. In *International Journal of Computer Vision*, volume 123, pp. 32–73. Springer, 2017.

Juncheng Li, Xin He, Longhui Wei, Long Qian, Linchao Zhu, Lingxi Xie, Yuetong Zhuang, Qi Tian, and Siliang Tang. Fine-grained semantically aligned vision-language pre-training. In *Advances in Neural Information Processing Systems*, 2022a.

Junnan Li, Ramprasaath Selvaraju, Akhilesh Gotmare, Shafiq Joty, Caiming Xiong, and Steven Chu Hong Hoi. Align before fuse: Vision and language representation learning with momentum distillation. *Advances in Neural Information Processing Systems*, 34:9694–9705, 2021a.

Junnan Li, Dongxu Li, Caiming Xiong, and Steven Hoi. Blip: Bootstrapping language-image pre-training for unified vision-language understanding and generation. In *International Conference on Machine Learning*, 2022b.

Junnan Li, Dongxu Li, Silvio Savarese, and Steven Hoi. Blip-2: Bootstrapping language-image pre-training with frozen image encoders and large language models. In *International Conference on Machine Learning*, 2023a.

Liunian Harold Li, Mark Yatskar, Da Yin, Cho-Jui Hsieh, and Kai-Wei Chang. What does bert with vision look at? In *Proceedings of the 58th Annual Meeting of the Association for Computational Linguistics*, pp. 5265–5275, 2020a.

Liunian Harold Li, Pengchuan Zhang, Haotian Zhang, Jianwei Yang, Chunyuan Li, Yiwu Zhong, Lijuan Wang, Lu Yuan, Lei Zhang, Jenq-Neng Hwang, et al. Grounded language-image pre-training. In *Proceedings of the IEEE/CVF Conference on Computer Vision and Pattern Recognition*, pp. 10965–10975, 2022c.

Manling Li, Ruochen Xu, Shuohang Wang, Luowei Zhou, Xudong Lin, Chenguang Zhu, Michael Zeng, Heng Ji, and Shih-Fu Chang. Clip-event: Connecting text and images with event structures. In *Proceedings of the IEEE/CVF Conference on Computer Vision and Pattern Recognition*, pp. 16420–16429, 2022d.

Xiujun Li, Xi Yin, Chunyuan Li, Pengchuan Zhang, Xiaowei Hu, Lei Zhang, Lijuan Wang, Houdong Hu, Li Dong, Furu Wei, et al. Oscar: Object-semantics aligned pre-training for vision-language tasks. In *European Conference on Computer Vision*, pp. 121–137. Springer, 2020b.

Yangguang Li, Feng Liang, Lichen Zhao, Yufeng Cui, Wanli Ouyang, Jing Shao, Fengwei Yu, and Junjie Yan. Supervision exists everywhere: A data efficient contrastive language-image pre-training paradigm. In *International Conference on Learning Representations*, 2021b.

Yanghao Li, Haoqi Fan, Ronghang Hu, Christoph Feichtenhofer, and Kaiming He. Scaling language-image pre-training via masking. In Proceedings of the IEEE/CVF Conference on Computer Vision and Pattern Recognition, pp. 23390–23400, 2023b.

Tsung-Yi Lin, Michael Maire, Serge Belongie, James Hays, Pietro Perona, Deva Ramanan, Piotr Dollár, and C Lawrence Zitnick. Microsoft coco: Common objects in context. In European Conference on Computer Vision, pp. 740–755. Springer, 2014.

Yinhan Liu, Myle Ott, Naman Goyal, Jingfei Du, Mandar Joshi, Danqi Chen, Omer Levy, Mike Lewis, Luke Zettlemoyer, and Veselin Stoyanov. Roberta: A robustly optimized bert pretraining approach. arXiv preprint arXiv:1907.11692, 2019.

Ze Liu, Yutong Lin, Yue Cao, Han Hu, Yixuan Wei, Zheng Zhang, Stephen Lin, and Baining Guo. Swin transformer: Hierarchical vision transformer using shifted windows. In International Conference on Computer Vision, pp. 10012–10022, 2021.

Ilya Loshchilov and Frank Hutter. Sgdr: Stochastic gradient descent with warm restarts. arXiv preprint arXiv:1608.03983, 2016.

Jiasen Lu, Dhruv Batra, Devi Parikh, and Stefan Lee. Vilbert: Pretraining task-agnostic visiolinguistic representations for vision-and-language tasks. Advances in Neural Information Processing Systems, 32, 2019.

Zhiyuan Ma, Jianjun Li, Guohui Li, and Kaiyan Huang. Cmal: A novel cross-modal associative learning framework for vision-language pre-training. In Proceedings of the 30th ACM International Conference on Multimedia, pp. 4515–4524, 2022.

Youssef Mroueh, Chun-Liang Li, Tom Sercu, Anant Raj, and Yu Cheng. Sobolev gan. In International Conference on Learning Representations, 2018.

Youssef Mroueh, Tom Sercu, and Anant Raj. Sobolev descent. In International Conference on Artificial Intelligence and Statistics, pp. 2976–2985. PMLR, 2019.

Norman Mu, Alexander Kirillov, David A. Wagner, and Saining Xie. Slip: Self-supervision meets language-image pre-training. arXiv, abs/2112.12750, 2021.

Aaron van den Oord, Yazhe Li, and Oriol Vinyals. Representation learning with contrastive predictive coding. arXiv preprint arXiv:1807.03748, 2018.

Richard Yuanzhe Pang and He He. Text generation by learning from demonstrations. In International Conference on Learning Representations, 2021.

Kishore Papineni, Salim Roukos, Todd Ward, and Wei-Jing Zhu. Bleu: a method for automatic evaluation of machine translation. In Proceedings of the 40th Annual Meeting of the Association for Computational Linguistics, pp. 311–318, 2002.

Jaeyoo Park and Bohyung Han. Multi-modal representation learning with text-driven soft masks. In Proceedings of the IEEE/CVF Conference on Computer Vision and Pattern Recognition, pp. 2798–2807, 2023.

Gabriel Peyré, Marco Cuturi, and Justin Solomon. Gromov-wasserstein averaging of kernel and distance matrices. In International Conference on Machine Learning, pp. 2664–2672. PMLR, 2016.

Gabriel Peyré, Marco Cuturi, et al. Computational optimal transport: With applications to data science. Foundations and Trends® in Machine Learning, 11(5-6):355–607, 2019.

Bryan A Plummer, Liwei Wang, Chris M Cervantes, Juan C Caicedo, Julia Hockenmaier, and Svetlana Lazebnik. Flickr30k entities: Collecting region-to-phrase correspondences for richer image-to-sentence models. In International Conference on Computer Vision, pp. 2641–2649, 2015.

Shraman Pramanick, Aniket Roy, and Vishal M Patel. Multimodal learning using optimal transport for sarcasm and humor detection. In Proceedings of the IEEE/CVF Winter Conference on Applications of Computer Vision, pp. 3930–3940, 2022.

Shraman Pramanick, Yale Song, Sayan Nag, Kevin Qinghong Lin, Hardik Shah, Mike Zheng Shou, Rama Chellappa, and Pengchuan Zhang. Egovlpv2: Egocentric video-language pre-training with fusion in the backbone. arXiv preprint arXiv:2307.05463, 2023.

Alec Radford, Jeff Wu, Rewon Child, David Luan, Dario Amodei, and Ilya Sutskever. Language models are unsupervised multitask learners. 2019.

Alec Radford, Jong Wook Kim, Chris Hallacy, Aditya Ramesh, Gabriel Goh, Sandhini Agarwal, Girish Sastry, Amanda Askell, Pamela Mishkin, Jack Clark, et al. Learning transferable visual models from natural language supervision. In International Conference on Machine Learning, pp. 8748–8763. PMLR, 2021.

Shaoqing Ren, Kaiming He, Ross Girshick, and Jian Sun. Faster r-cnn: Towards real-time object detection with region proposal networks. Advances in Neural Information Processing Systems, 28, 2015.

Anshul Shah, Suvrit Sra, Rama Chellappa, and Anoop Cherian. Max-margin contrastive learning. In Proceedings of the AAAI Conference on Artificial Intelligence, volume 36, pp. 8220–8230, 2022.

Amanpreet Singh, Ronghang Hu, Vedanuj Goswami, Guillaume Couairon, Wojciech Galuba, Marcus Rohrbach, and Douwe Kiela. Flava: A foundational language and vision alignment model. In Proceedings of the IEEE/CVF Conference on Computer Vision and Pattern Recognition, pp. 15638–15650, 2022.

Weijie Su, Xizhou Zhu, Yue Cao, Bin Li, Lewei Lu, Furu Wei, and Jifeng Dai. Vi-bert: Pre-training of generic visual-linguistic representations. In International Conference on Learning Representations, 2019.

Alane Suhr, Stephanie Zhou, Ally Zhang, Iris Zhang, Huajun Bai, and Yoav Artzi. A corpus for reasoning about natural language grounded in photographs. In Proceedings of the Annual Meeting of the Association for Computational Linguistics, 2019.

Hao Tan and Mohit Bansal. Lxmert: Learning cross-modality encoder representations from transformers. In Proceedings of the 2019 Conference on Empirical Methods in Natural Language Processing and the 9th International Joint Conference on Natural Language Processing, pp. 5100–5111, 2019.

Ramakrishna Vedantam, C Lawrence Zitnick, and Devi Parikh. Cider: Consensus-based image description evaluation. In Proceedings of the IEEE Conference on Computer Vision and Pattern Recognition, pp. 4566–4575, 2015.

Jianfeng Wang, Zhengyuan Yang, Xiaowei Hu, Linjie Li, Kevin Lin, Zhe Gan, Zicheng Liu, Ce Liu, and Lijuan Wang. Git: A generative image-to-text transformer for vision and language. Transactions of Machine Learning Research, 2023a.

Jinpeng Wang, Pan Zhou, Mike Zheng Shou, and Shuicheng Yan. Position-guided text prompt for vision-language pre-training. In Proceedings of the IEEE/CVF Conference on Computer Vision and Pattern Recognition, pp. 23242–23251, 2023b.

Junke Wang, Dongdong Chen, Zuxuan Wu, Chong Luo, Luowei Zhou, Yucheng Zhao, Yujia Xie, Ce Liu, Yu-Gang Jiang, and Lu Yuan. Omnil: One foundation model for image-language and video-language tasks. In Advances in Neural Information Processing Systems, 2022a.

Peng Wang, An Yang, Rui Men, Junyang Lin, Shuai Bai, Zhikang Li, Jianxin Ma, Chang Zhou, Jingren Zhou, and Hongxia Yang. Ofa: Unifying architectures, tasks, and modalities through a simple sequence-to-sequence learning framework. In International Conference on Machine Learning, pp. 23318–23340. PMLR, 2022b.

Teng Wang, Yixiao Ge, Feng Zheng, Ran Cheng, Ying Shan, Xiaohu Qie, and Ping Luo. Accelerating vision-language pretraining with free language modeling. In Proceedings of the IEEE/CVF Conference on Computer Vision and Pattern Recognition, pp. 23161–23170, 2023c.

Wenhui Wang, Hangbo Bao, Li Dong, and Furu Wei. Vlmo: Unified vision-language pre-training with mixture-of-modality-experts. arXiv preprint arXiv:2111.02358, 2021a.

Wenhui Wang, Hangbo Bao, Li Dong, Johan Bjorck, Zhiliang Peng, Qiang Liu, Kriti Aggarwal, Owais Mohammed, Saksham Singhal, Subhajit Som, and Furu Wei. Image as a foreign language: Beit pretraining for all vision and vision-language tasks. arXiv, abs/2208.10442, 2022c.

Wenhui Wang, Hangbo Bao, Li Dong, Johan Bjorck, Zhiliang Peng, Qiang Liu, Kriti Aggarwal, Owais Khan Mohammed, Saksham Singhal, Subhajit Som, et al. Image as a foreign language: Beit pretraining for vision and vision-language tasks. In Proceedings of the IEEE/CVF Conference on Computer Vision and Pattern Recognition, pp. 19175–19186, 2023d.

Zirui Wang, Jiahui Yu, Adams Wei Yu, Zihang Dai, Yulia Tsvetkov, and Yuan Cao. Simvlm: Simple visual language model pretraining with weak supervision. In International Conference on Learning Representations, 2021b.

Jason Wei and Kai Zou. Eda: Easy data augmentation techniques for boosting performance on text classification tasks. In Proceedings of the 2019 Conference on Empirical Methods in Natural Language Processing and the 9th International Joint Conference on Natural Language Processing, pp. 6382–6388, 2019.

Yuxin Wu, Alexander Kirillov, Francisco Massa, Wan-Yen Lo, and Ross Girshick. Detectron2. <https://github.com/facebookresearch/detectron2>, 2019.

Hongwei Xue, Yupan Huang, Bei Liu, Houwen Peng, Jianlong Fu, Houqiang Li, and Jiebo Luo. Probing inter-modality: Visual parsing with self-attention for vision-and-language pre-training. Advances in Neural Information Processing Systems, 34:4514–4528, 2021.

Jianwei Yang, Chunyuan Li, Pengchuan Zhang, Bin Xiao, Ce Liu, Lu Yuan, and Jianfeng Gao. Unified contrastive learning in image-text-label space. In Proceedings of the IEEE/CVF Conference on Computer Vision and Pattern Recognition, pp. 19163–19173, 2022a.

Jinyu Yang, Jiali Duan, Son Tran, Yi Xu, Sampath Chanda, Liqun Chen, Belinda Zeng, Trishul Chilimbi, and Junzhou Huang. Vision-language pre-training with triple contrastive learning. In Proceedings of the IEEE/CVF Conference on Computer Vision and Pattern Recognition, pp. 15671–15680, 2022b.

Zhengyuan Yang, Zhe Gan, Jianfeng Wang, Xiaowei Hu, Faisal Ahmed, Zicheng Liu, Yumao Lu, and Lijuan Wang. Unitab: Unifying text and box outputs for grounded vision-language modeling. In European Conference on Computer Vision, 2022c.

Lewei Yao, Runhui Huang, Lu Hou, Guansong Lu, Minzhe Niu, Hang Xu, Xiaodan Liang, Zhenguo Li, Xin Jiang, and Chunjing Xu. Filip: Fine-grained interactive language-image pre-training. In International Conference on Learning Representations, 2022.

Haoxuan You, Luwei Zhou, Bin Xiao, Noel Codella, Yu Cheng, Ruochen Xu, Shih-Fu Chang, and Lu Yuan. Learning visual representation from modality-shared contrastive language-image pre-training. In European Conference on Computer Vision, 2022.

Yang You, Igor Gitman, and Boris Ginsburg. Large batch training of convolutional networks. arXiv preprint arXiv:1708.03888, 2017.

Licheng Yu, Patrick Poirson, Shan Yang, Alexander C Berg, and Tamara L Berg. Modeling context in referring expressions. In European Conference on Computer Vision, pp. 69–85. Springer, 2016.

Siyang Yuan, Ke Bai, Liqun Chen, Yizhe Zhang, Chenyang Tao, Chunyuan Li, Guoyin Wang, Ricardo Henao, and Lawrence Carin. Advancing weakly supervised cross-domain alignment with optimal transport. In British Machine Vision Conference, 2020.

Xin Yuan, Zhe Lin, Jason Kuen, Jianming Zhang, Yilin Wang, Michael Maire, Ajinkya Kale, and Baldo Faieta. Multimodal contrastive training for visual representation learning. In Proceedings of the IEEE/CVF Conference on Computer Vision and Pattern Recognition, pp. 6995–7004, 2021.

Jure Zbontar, Li Jing, Ishan Misra, Yann LeCun, and Stéphane Deny. Barlow twins: Self-supervised learning via redundancy reduction. In International Conference on Machine Learning, pp. 12310–12320. PMLR, 2021.

Yan Zeng, Xinsong Zhang, and Hang Li. Multi-grained vision language pre-training: Aligning texts with visual concepts. In International Conference on Machine Learning, 2022.

Chi Zhang, Yujun Cai, Guosheng Lin, and Chunhua Shen. Deepemd: Few-shot image classification with differentiable earth mover’s distance and structured classifiers. In Proceedings of the IEEE/CVF Conference on Computer Vision and Pattern Recognition, pp. 12203–12213, 2020.

Haotian Zhang, Pengchuan Zhang, Xiaowei Hu, Yen-Chun Chen, Liunian Harold Li, Xiyang Dai, Lijuan Wang, Lu Yuan, Jenq-Neng Hwang, and Jianfeng Gao. Glipv2: Unifying localization and vision-language understanding. Advances in Neural Information Processing Systems, 2022.

Pengchuan Zhang, Xiuju Li, Xiaowei Hu, Jianwei Yang, Lei Zhang, Lijuan Wang, Yejin Choi, and Jianfeng Gao. Vinvl: Revisiting visual representations in vision-language models. In Proceedings of the IEEE/CVF Conference on Computer Vision and Pattern Recognition, pp. 5579–5588, 2021.

Luowei Zhou, Hamid Palangi, Lei Zhang, Houdong Hu, Jason Corso, and Jianfeng Gao. Unified vision-language pre-training for image captioning and vqa. In Proceedings of the AAAI Conference on Artificial Intelligence, volume 34, pp. 13041–13049, 2020.

A Pesudo Code of VoLTA

The training pseudo code for VoLTA is as follows:

Algorithm 1 PyTorch-style pseudocode for VoLTA.

```

# f_I: Image Encoder, f_T: Text Encoder
# task_names: string containing task names
# I: Image input, T: Text input, N: Batch size, D: Projector dim
# BT: Barlow Twins loss function
# WD, GWD: Wasserstein and Gromov-Wasserstein loss functions
# MLM, ITM: MLM and ITM loss functions, respectively
# gamma: coefficient of GWD loss in GOT
# w_GOT: weight of GOT loss

def GOT(x_1, x_2, f_1, f_2):
    # compute embeddings
    z_A, z_B = f_1(x_1), f_2(x_2) # N x D

    # normalize representation along batch dimension
    z_A_norm = (z_A - z_A.mean(dim=0)) / z_A.std(dim=0)
    z_B_norm = (z_B - z_B.mean(dim=0)) / z_B.std(dim=0)

    # cosine distance matrix
    c = cosine_dist_matrix(z_A, z_B)
    # Wasserstein distance
    loss_w = W_D(c, z_A.size(0), z_A.size(1), z_B.size(1))
    # Gromov-Wasserstein distance
    loss_gw = GW_D(z_A.transpose(2,1), z_B.transpose(2,1))

    return gamma * torch.mean(loss_gw) + (1 - gamma) * torch.mean(loss_w)

def VoLTA (I, T):
    total_loss = torch.tensor(0.)
    for x in loader: # load a batch with N samples
        # two augmented versions of I, T
        I1, I2 = augment_image(I); T1, T2 = augment_text(T)

        if "BTGOT" in task_names:
            # BT loss
            intra_loss = BT(I1, I2, f_I) + BT(T1, T2, f_T)
            inter_loss = BT(I1, T1, f_I, f_T) + BT(I2, T2, f_I, f_T)
            BT_loss = intra_loss + inter_loss
            total_loss += BT_loss

            # GOT loss
            GOT_loss = GOT(I1, T1, f_I, f_T) + GOT(I2, T2, f_I, f_T)
            total_loss += w_GOT * GOT_loss

        # cross-attention is enabled
        if "MLM" in task_names:

            # MLM loss
            MLM_loss = MLM(T1, I1, mask_T1, f_I, f_T)
            total_loss += MLM_loss

        if "ITM" in task_names:

            # ITM loss
            ITM_loss = ITM(T1, I1, false_image_1, f_I, f_T)
            total_loss += ITM_loss

    return total_loss

```

B Overview of Vision-Language Pre-training Models

Vision-Language Pre-trained (VLP) models have proven extremely beneficial for multi-modal tasks in recent years. Earlier works were predominantly focused on using pre-trained object detectors to extract patch

Model	Venue	Vision Encoder	Text Enc.	Multimodality Fusion	Pre-train I-T	I-T-B	Pre-training Objectives
ViLBERT	NeurIPS'19	OD+Xformer	Xformer	Co-attn	✓		MLM+ITM+MIM
LXMERT	EMNLP'19				✓		MLM+ITM+MIM+VQA
VisualBERT	ACL'20				✓		MLM+ITM
VL-BERT	ICLR'20				✓		MLM+MIM
UNITER	ECCV'20				✓		MLM+ITM+MIM+WRA
OSCAR	ECCV'20				✓		MLM+ITM
VinVL	CVPR'21				✓		MLM+ITM
VL-T5	ICML'21					✓	MLM+ITM+VQA+Grnd+Cap
SOHO	CVPR'21				✓		MLM+ITM+MIM
SimVLM	ICLR'22				✓		PrefixLM
MDETR	ICCV'21					✓	OD+TP+CA
ViT	ICML'21				✓		MLM+ITM
Visual Parsing	NeurIPS'21				✓		MLM+ITM+MIM
ALBEF	NeurIPS'21				✓		MLM+ITM+ITC
METER	CVPR'22				✓		MLM+ITM
CLIP	ICML'21	CNN/Xformer		None	✓		ITC
DeCLIP	ICLR'21				✓		ITC+MLM+SL+MVS+NNS
ALIGN	ICML'21	CNN			✓		ITC
GLIP	CVPR'22				✓	✓	OD+CE+WRA
GLIPv2	NeurIPS'22	OD+Xformer			✓	✓	OD+CE+WRA+MLM
BLIP	ICML'22			Cross-modality MHA	✓		ITC+ITM+LM
OmniVL	NeurIPS'22				✓		UniVLC+VLM+LM
X-VLM	ICML'22	Xformer			✓	✓	BBP+ITC+MP+MLM
CMAL	ACM MM'22				✓		AMC+MLM+MRM+ITM+ITC
LOUPE	NeurIPS'22			None	✓		ITC+FSA+TSA
FILIP	ICLR'22				✓		ITC
UniCL	CVPR'22	CNN/Xformer			✓		ITC
UniTAB	ECCV'22	CNN			✓		LM
TCL	CVPR'22			Merged attn	✓	✓	CMA+IMC+LMI+ITM+MLM
MS-CLIP	ECCV'22			Shared Attention	✓		ITC
FLM	CVPR'23	Xformer		Cross-modality MHA	✓		FLM + ITM
BLIP-2	ICML'23			Cross-modality Adaptive Attention	✓		ITC+ITM+ITG
Fame-ViL	CVPR'23			Cross-modality MHA	✓		ITC
PTP	CVPR'23	OD+Xformer		Merged attn	✓		ITC+ITM+LM
Softmask++	CVPR'23			Unified attn	✓		ITC+ITM+MLM
OneR	AAAI'23			Shared MHA	✓		ITC+XMC+CIC+CMC
BEiT-3	CVPR'23	Xformer		None	✓		MDM
FLIP	CVPR'23			Merged attn	✓		ITC
GIT	TMLR'23		Emb.		✓		LM
FIBER	NeurIPS'22	Xformer	Xformer	Merged Co-attn	✓	✓	MLM+ITM+ITC
VoLTA	TMLR'23	CNN/Xformer	Xformer	Merged Co-attn	✓		BT+GOT+MLM+ITM

Table B.1: **Overview of VLP models.** OD: objective detector. Xformer: transformer. Emb.: embedding. MLM/MIM: masked language/image modeling. ITM: image-text matching. WRA: word-region alignment. ITC: image-text contrastive learning. Grnd: Grounding. Cap: Captioning. TP: Token Prediction. CA: Contrastive Alignment, NNS: Nearest Neighbour Supervision, MVS: Multiview Supervision, SL: Sim-siam Loss, MHA: Multi-head attn., LM: Language Modeling, UniVLC: Unified Vision Language Contrastive, VLM: Vision Language Matching, BBP: Bounding Box Prediction, MP: Matching Prediction, FSA: Fine-grained Semantic Alignment, TSA: Token-level Semantic Alignment, AMC: Associative Mapping Classification, CMA: Cross-Modal Alignment, IMC: Intra-Modal Contrastive, LMI: Local Mutual Information Maximization, I-T: Image-Text, I-T-B: Image-Text-Box, ITG: Image grounded text generation, XMC: Cross-Modal Mixup Contrastive, CIC: Contextual Invariance Contrastive, CMC: Contextual Mixup Contrast, MDM: Masked Data Modeling.

(region) level information from corresponding images (Lu et al., 2019; Li et al., 2020a; Tan & Bansal, 2019; Chen et al., 2020d; Su et al., 2019). In some of these models, such as ViLBERT (Lu et al., 2019), and LXMERT (Tan & Bansal, 2019), multi-modality fusion has been achieved via co-attention using a third transformer which contains fused information independently obtained from respective vision and language encoders. On the contrary, VisualBERT (Li et al., 2020a), VL-BERT (Su et al., 2019), and UNITER (Chen et al., 2020d) employ a merged attention strategy to fuse both image patches and text features together into a unified transformer through corresponding image and text embedders. In addition to these, OSCAR (Li et al., 2020b) uses object tags as inputs. VinVL (Zhang et al., 2021) follows a similar strategy to that of OSCAR, the only difference being their novel 3-way contrastive loss which optimizes the training objectives used for VQA and text-image matching. VL-T5 (Cho et al., 2021) exploits bounding-box coordinate information,

image IDs, and region IDs along with ROI features for visual embedding. Here, encoded visual and textual features are fed into a bi-directional multi-modal encoder and an auto-regressive text decoder framework, respectively, for pre-training.

In all the above methods, pre-trained object detectors are kept frozen during the training. Furthermore, extracting region-level features from images can be tedious. To address these shortcomings, end-to-end pre-training methods have been developed. PixelBERT (Huang et al., 2020) uses a CNN-based vision encoder and sentence encoder to obtain image and text representations, respectively. These representations are subsequently fed into a transformer via a cross-modality alignment. SOHO (Huang et al., 2021) uses grid features-based discretization via a learned vision dictionary which is then fed into a cross-modal module. SimVLM (Wang et al., 2021b) uses CNN and text token embedding for image and text feature representation extraction with a unified encoder-decoder transformer trained on a PrefixLM objective. Finally, MDETR (Kamath et al., 2021) uses CNN and RoBERTa (along with corresponding projection layers) for image and text feature extraction. These extracted features are concatenated before passing through a unified transformer trained on 1.3M Image-Text-Box (I-T-B) annotated data.

In recent years, the rise of Vision Transformers (ViT) (Dosovitskiy et al., 2021) has motivated the research community to have an all-transformer framework by incorporating ViTs (instead of CNN backbones) in VLP models. Image patch features and text token embeddings are fed directly into a ViT model for pre-training in ViLT (Kim et al., 2021). Visual Parsing (Xue et al., 2021), ALBEF (Li et al., 2021a), and METER (Dou et al., 2022b) use ViTs as vision encoders for image feature generation. ALBEF and METER use co-attention in their pre-training frameworks for multimodality fusion.

Another class of VLP models in the form of CLIP (Radford et al., 2021), DeCLIP (Li et al., 2021b), and ALIGN (Jia et al., 2021) has been introduced lately. Although known for their impressive zero-shot recognition ability and excellent transferability to downstream tasks, these models typically rely on huge amounts of image-text pairs for pre-training. Contrastive loss forms the core component of the pre-training objectives in these VLP models. In such models (e.g., CLIP (Radford et al., 2021), DeCLIP (Li et al., 2021b)), separate encoders have been used for each modality. On the contrary, modality-shared contrastive language-image pre-training (MS-CLIP) (You et al., 2022) leverages knowledge distribution across multiple modalities (image and text) through parameter sharing. In their unified framework, the parameters which are being shared between two modalities include the attention and feedforward modules and the layerNorm layers.

GLIP (Li et al., 2022c) and GLIPv2 (Zhang et al., 2022) use a localization loss along with a word-region alignment loss for pre-training corresponding encoders using image-text-box annotations. BLIP (Li et al., 2022b) employs image and text encoders connected through a cross-modality multi-head attention which are pre-trained on image-text pairs using contrastive and language modeling objectives. OmniVL (Wang et al., 2022a) utilizes a unified image (and video) encoder and a text encoder pre-trained on image-text, image-label, video-text, and video-label pairs using unified vision-language contrastive, vision-language matching and language modeling losses. Furthermore, a visual-grounded alignment decoder is also present for facilitating better learning and alignment between various modalities. X-VLM (Zeng et al., 2022) employs a vision transformer to extract features from the subset of patches representing images/regions/objects. These patch features are then paired with associated text features for contrastive learning, matching, and masked language modeling. Additionally, image and text pairings are also done for bounding-box prediction which is used to locate visual concepts in the image. CMAL (Ma et al., 2022) proposes interactions between features (obtained from respective image and text encoders) via cross-modal associative mappings which help in fine-grained semantic alignment between the learned representations. LOUPE (Li et al., 2022a) implements token-level and semantics-level Shapley interaction modeling with global image-text contrastive loss (in a dual-encoder setting) for explicit learning of fine-grained semantic alignment between visual regions and textual phrases without using expensive bounding-box annotations. FILIP (Yao et al., 2022) removes the need for cross-modality attention fusion by modeling the fine-grained semantic alignment between visual and textual tokens via a novel cross-modal late interaction mechanism in contrastive loss. TCL (Yang et al., 2022b) uses global cross-modal alignment, intra-modal alignment, and local mutual information maximization losses along with masked language modeling and image-text matching to learn robust image-text representations during pre-training. UniCL (Yang et al., 2022a) utilizes a unified learning method with a two-way contrastive loss

(image-to-text and text-to-image) in the image-text-label space which can learn representations from either of the image-label and image-text data or both. UniTAB (Yang et al., 2022c) employs a transformer-based encoder-decoder framework that can jointly output open-ended text and box, encouraging alignment between words and boxes.

In order to accelerate the convergence of VL pretraining, Wang et al. (2023c) proposed free language modeling (FLM) which addresses the issues inherent to masked language modeling (MLM) and autoregressive modeling. Using FLM as a pre-training objective, the authors have achieved impressive performance on several downstream tasks. Fame-ViL (Han et al., 2023) introduces a parameter-efficient VLP approach employing a task-versatile architecture with cross-attention and task-specific adapters. Fame-ViL applies a single model for various heterogeneous fashion tasks achieving performance gains over previous SOTA benchmarks. Wang et al. (2023b) have introduced a simple yet effective position-guided text prompt (PTP) paradigm to improve the visual grounding capability of existing cross-modal VL architectures and help them better handle various downstream tasks. Park & Han (2023) have proposed a VL framework based on the explainable soft feature masking and regularization via diversification strategies for improving the performance of VL models in several downstream tasks. Li et al. (2023a) have devised BLIP-2, where a lightweight querying transformer is pre-trained using a two-stage strategy to bridge the modality gap. A frozen encoder is used in the first stage to bootstrap VL representation learning, and vision-to-language generative learning is bootstrapped in the second stage employing a frozen LLM, allowing zero-shot generation capabilities. Jang et al. (2023) have developed a simple and unified VL model (as a single tower) in a modality-agnostic manner. BEiT-3 (Wang et al., 2023d) introduces a general-purpose multimodal foundation model to pre-train a multiway transformer by performing masked data modeling on inputs irrespective of modalities (i.e., images, texts, and image-text pairs). FLIP (Li et al., 2023b) extends CLIP (Radford et al., 2021) by performing contrastive learning on pairs of masked image patches and corresponding texts without reconstructing the masked image content. GIT (Wang et al., 2023a) unifies the VL architecture (an image encoder and a text decoder) under a single language modeling task while also scaling up the pre-training data and the model size to gain superior performance on captioning and question-answering downstream tasks.

FIBER (Dou et al., 2022a) fuses vision and language encoder backbones through merged co-attention which are then pre-trained on 4M data with two-stage pre-training (coarse- and fine-grained). Image-text pairs are used in the coarse-grained pre-training stage which is then followed by a fine-grained pre-training stage with image-text-box annotations. However, these bounding box annotations come with extra overheads. Therefore, in our model, VOLTA, we propose an alternate solution for optimal-transport based local feature-level alignment using global image-caption annotations which performs well not only on coarse-grained tasks (such as VQA and Image Captioning), but also on fine-grained tasks (such as Referring Expression Comprehension and Object Detection). Table B.1 encapsulates an overview of the details of all these aforementioned methods.

C Downstream Datasets

Our downstream tasks can be categorized into three groups: uni-modal, multi-modal coarse-grained, and multi-modal fine-grained.

Uni-modal: For uni-modal tasks, we fine-tune (and validate) our pre-trained model on ImageNet-1k (Deng et al., 2009) for image classification, VOC07+12 (Everingham et al., 2010) for image classification and object detection, and COCO (Lin et al., 2014) for image classification, object detection, and instance segmentation.

Multi-modal Coarse-grained: Here, we fine-tune (and validate) our pre-trained model on VQAv2 (Antol et al., 2015) for visual question answering, NLVR² (Suhr et al., 2019) for visual reasoning, Flickr30k (Plummer et al., 2015) for image and text retrieval, and COCO (Lin et al., 2014) for image captioning.

Multi-modal Fine-grained: For these tasks, we fine-tune (and validate) our pre-trained model on RefCOCO, RefCOCO+, and RefCOCOg (Kazemzadeh et al., 2014; Yu et al., 2016) for referring expression comprehension, and COCO (Lin et al., 2014) and LVIS Mini (Gupta et al., 2019) for language-conditioned object detection.

Modality	Task	Dataset	Image Src	#Images	#Text	Metric
Uni-modal	Image Classfn.	IN-1K	IN-1K	1.3M	-	Accuracy
		COCO	COCO	123K	-	F1
		VOC07+12	VOC07+12	16K	-	mAP
	Object Det.	COCO	COCO	123K	-	AP ^{bb}
		VOC07+12	VOC07+12	16K	-	AP ^{mk}
	Instance Seg.	COCO	COCO	123K	-	AP ^{mk}
Multi-modal coarse-grained	VQA	VQA	COCO	204K	1.1M	VQA-Score
	NLVR ²	NLVR ²	Web Crawled	214K	107K	Accuracy
	IR-TR	Flickr30K	Flickr30K	32K	160K	Recall@1
	Captioning	COCO	COCO	123K	615K	B@4,M,C,S
	Ref. Exp. Comp.	RefCOCO	COCO	20K	142K	Accuracy
Multi-modal fine-grained	Ref. Exp. Comp.	RefCOCO+	COCO	20K	142K	Accuracy
		RefCOCOg	COCO	26K	95K	AP
	Mul. Obj. Det.	LVIS Mini	COCO	123K	615K	AP

Table C.1: **Dataset statistics for uni-modal and multi-modal downstream tasks.**

Several multi-modal downstream tasks are built based on the COCO dataset, where the validation and test splits of these downstream tasks are scattered across the raw COCO splits. Therefore, during pre-training, we carefully selected the portion of the COCO dataset which does not overlap with the validation/test splits of these multi-modal downstream tasks.

D Implementation Details & Hyper-parameter Values

D.1 Data Augmentation

We use ResNet50/Swin-T/Swin-B (He et al., 2016; Liu et al., 2021) as image encoder and RoBERTa (Liu et al., 2019) as text encoder. Each encoder is followed by a projector network which is a 3-layer MLP with the configuration [d-2048-2048-1024]. Here, d represents the embedding dimension of the encoder’s output.

Data Type	View #	Augmentation	Probability
Image	1	RandomResizedCrop	1.0
	1	RandomHorizontalFlip	0.5
	1	ColorJitter	0.8
	1	RandomGrayscale	0.2
	1	GaussianBlur	1.0
	1	Solarization	0.0
	2	RandomResizedCrop	1.0
	2	RandomHorizontalFlip	0.5
	2	ColorJitter	0.8
	2	RandomGrayscale	0.2
	2	GaussianBlur	0.1
	2	Solarization	0.2
Text	1	Synonym Replacement	0.1
	1	Random Insertion	0.1
	1	Random Swap	0.1
	1	Random Deletion	0.1
	2	Synonym Replacement	0.1
	2	Random Insertion	0.2
	2	Random Swap	0.1
	2	Random Deletion	0.2

Table D.1: **Image and text augmentation details.**

Image Augmentations: Two sets of random transformations sampled from an augmentation pool are applied on each input image to generate two disparate distorted views. The augmentation policy is composed of `RandomResizedCrop`, `RandomHorizontalFlip`, `ColorJitter`, `RandomGrayscale`, `GaussianBlur`, and `Solarization` augmentations. `RandomResizedCrop` is applied with a probability of 1.0, whereas the remaining ones are applied randomly with varying probabilities following Zbontar et al. (2021) (see Table D.1).

Text Augmentations: Two sets of random transformations are applied on input text using EDA (Wei & Zou, 2019) including synonym replacement, random insertion, random swap, and random deletion with different probabilities as outlined in Table D.1.

D.2 Pre-training Setup

Table D.2 shows the details of hyper-parameters used during training.

VoLTA comprises a vision encoder and a language encoder with a merged co-attention for cross-modality fusion. In our experiments, we have considered two types of vision encoder backbones - ResNet-50 (He et al., 2016) and Swin Transformer (Liu et al., 2021). For fair comparisons with related works (Dou et al., 2022b;a), the input image resolution for ResNet-50 encoder backbone is kept as 224×224 , whereas for Swin-B, it is 384×384 . The output embedding dimension of the image encoder in both cases is 1024. Similarly, to be consistent with Dou et al. (2022b;a), we have selected RoBERTa as the language encoder with a vocabulary size of 50265, a tokenizer as ‘roberta-base’, a maximum input text length of 30, and an output embedding dimension of 768 (please refer to Table D.2 for more details).

Separate projector heads follow vision and language encoders. A projector head consists of 3 linear layers, each with 2048 output units (except for the last one, which has 1024 output units), followed by a Batch Normalization layer and ReLU activation (for exact configuration, please refer to Table D.2). The final projected output denotes the input (image/text) feature representation used in downstream tasks. The embeddings (i.e., output from respective encoders) are fed into the loss function of VoLTA to learn these representations.

The loss function of VoLTA includes four different loss components, namely, multi-modal Barlow Twins for intra- and inter-modality redundancy reduction, GOT for alignment of local features, and MLM and ITM together for encouraging cross-modal attention fusion. For MLM, we randomly mask 15%² (MLM probability in Table D.2) of the input tokens, and the model is trained to reconstruct the original tokens. For ITM, the model predicts whether a given image-text pair is matched.

For optimization, we follow the same protocol as described in Zbontar et al. (2021), where we use the LARS (You et al., 2017) optimizer to train our model for 20 epochs with a batch size of 256. A base LR of 0.1 is used for the weights and 0.0048 for the biases and batch normalization parameters which are then multiplied by a factor of 2. We employ a learning rate warm-up (linear) up to a period of 2 epochs followed by a cosine decay schedule to reduce the LR by a factor of 1000. A weight decay parameter 1e-6 is used, excluding the biases and batch normalization parameters. We conduct a grid search for the GOT loss hyperparameter (w_{GOT}), and we empirically found the best value to be 100.

Pre-training Cost: Our Swin-B backbone takes 6 hours per epoch to train on 64 V100 GPUs, with per GPU batch-size of 4.

D.3 Downstream Setup

D.3.1 Uni-modal downstream tasks

Linear Evaluation: For ImageNet, the linear classifier has been trained for 100 epochs with a batch size of 256, an LR of 0.3, and a cosine LR schedule. Cross-entropy loss is minimized with SGDM optimizer (momentum of 0.9), and a weight decay of 1e-6. For both COCO and VOC, the linear classifier has been trained for 100 epochs with AdamW optimizer with batch size of 256, an LR of 5e-2, and a weight decay of 1e-6.

Object Detection: For training the detection model, the detectron2 library (Wu et al., 2019) has been used. The backbone networks for Faster R-CNN (Ren et al., 2015) and Mask R-CNN (He et al., 2017) has been initialized using our pre-trained model.

For VOC07+12, we used the `trainval` set comprising 16K images for training a Faster R-CNN (Ren et al., 2015) C-4 backbone for 24K iterations using a batch size of 16 across 8 GPUs (using SyncBatchNorm). The

²Following BERT, we decompose this 15% into 10% random words, 10% unchanged, and 80% with a special token [MASK].

Hyper-parameters	Notation	Value
Model		
Img. proj. layer config.	-	$[d_i - 2048 - 2048 - 1024]$
Img. embed. dim	d_i	1024
Img. reso. (RN-50 & Swin-T)	-	224×224
Img. reso. (Swin-B)	-	384×384
Txt. proj. layer config.	-	$[d_t - 2048 - 2048 - 1024]$
Txt. embed. dim	d_t	768
Tokenizer	-	'roberta-base'
Vocab size	-	50265
MLM prob.	-	0.15
Max. length of text	-	30
# Heads of Xformer	-	12
# Layers of Xformer	-	12
# Fusion block	-	6
Dropout rate	-	0.1
Task names	-	'BTGOT, MLM, ITM'
Training		
Batch size	-	256
Epochs	-	20
Lambda_BT	λ	0.005
WD and GWD loss weight	γ	0.1
GOT loss weight	w_{GOT}	100.0
Optimizer	-	LARS
Base LR for weights	-	0.1
Base LR for biases	-	0.0048
Momentum	-	0.9
LR scheduler	-	Cosine LR decay (with linear warm-up)
Warm-up steps	-	$2 \times \text{Epochs}$
Weight decay	-	1e-6
End LR factor	-	0.001
Cosine LR amplitude factor	-	0.5

Table D.2: Pre-training hyper-parameter details for VoLTA.

initial learning rate for the model is 0.15, which is reduced by a factor of 10 after 18K and 22K iterations. Linear warmup (Goyal et al., 2017) is used with a slope of 0.333 for 1000 iterations.

For COCO, Mask R-CNN (He et al., 2017) with a C-4 backbone on the COCO 2017 train split is used for training, and the results are reported on the val split. A learning rate of 0.03 is used, and other parameters are kept the same as in the $1 \times$ schedule in detectron2 (Wu et al., 2019).

D.3.2 Coarse-grained multi-modal downstream tasks

Vision-Language Classification (VQAv2 and NLVR²): Vision-Language Classification task encompasses VQAv2 and NLVR², whose hyper-parameter setup has been taken from METER (Dou et al., 2022b) and FIBER (Dou et al., 2022a). Model finetuning is done with peak learning rates of 2e-5 for the backbones, 1e-4 for the cross-modal parameters, and 1e-3 for the head layer for 10 epochs with a batch size of 512. The image resolutions are set to 576 for VQAv2 and 384 for NLVR² and the models are evaluated with the VQA-Scores for VQAv2 and accuracy for NLVR² (Table C.1).

Image-Text Retrieval (IRTR): We follow Dou et al. (2022a) for IR-TR setup for the Flickr30k dataset, where the cross-attention layers in the backbones are removed during IR-TR fine-tuning and evaluation. The peak learning rates are set to 2e-5 for the backbones, and 1e-4 for the head layer. Furthermore, a batch size of 1024 is considered, and each image resolution is set to 576. We evaluate the Recall@1 metric for both the text and image retrieval tasks as outlined in Table C.1.

Image Captioning: For image captioning, only the image-to-text attentions are kept for the cross-modality attention fusion, and the model is converted into a standard seq2seq model (Dou et al., 2022a). We used a causal mask on the decoding side, and the outputs are predicted auto-regressively (Dou et al., 2022a).

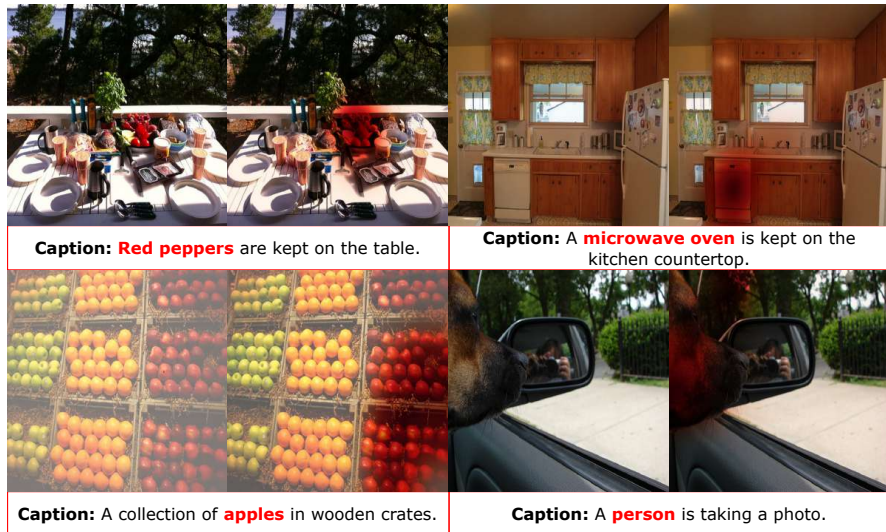


Figure E.1: **Limitations of our method:** tiny and hindered objects in cluttered environments are not distinctly attended by VoLTA. We look at the optimal transport plan from GOT to represent the alignment between the words in red with the corresponding input image. The visualizations are generated with 224p images, resulting in sequences of 196 tokens for 16×16 patches. All image-caption pairs are taken from the COCO2017 train split.

Models are trained with the cross-entropy loss for 5 epochs with the peak learning rates of 5e-5 for the backbones, and 2.5e-4 for the rest of the parameters, followed by a two-stage finetuning. In the first stage, finetuning with GOLD (Pang & He, 2021) is done for 5 epochs with a peak learning rate of 1e-5 for the backbones, since it is efficient and has been proven to be effective when the model input can correspond to different outputs. The second stage of fine-tuning involves CIDEr optimization where the learning rate is further reduced to 1e-6, and the model is trained for 3 epochs. A batch size of 512 is considered in both these cases, and a beam size of 5 is used during inference. Evaluation metrics include BLEU (Papineni et al., 2002), METEOR (Banerjee & Lavie, 2005), CIDEr (Vedantam et al., 2015), and SPICE (Anderson et al., 2016) scores (shown in Table C.1).

D.3.3 Fine-grained multi-modal downstream tasks

Referring Expression Comprehension (REC): We follow Dou et al. (2022a) for training and evaluation on 3 different datasets (RefCOCO, RefCOCO+, and RefCOCO) where the models are finetuned with a batch size of 16 for 20 epochs. A warmup of 2000 steps with a peak LR of 1e-5 is used for the OD head as well as the rest of the model’s parameters. LR drops twice, once at 67% and the other at 89% of the total number of steps. Horizontal flip augmentation has been turned off during REC training because it was observed by Dou et al. (2022a) that horizontal flip adversely affected the performance, particularly on the RefCOCO dataset. Accuracy is used as the evaluation metric in this case (Table C.1).

Object Detection: We follow the training and evaluation setup of Dou et al. (2022a) for text-conditioned (multi-modal) object detection. For both COCO and LVIS datasets, the model has been finetuned for 24 epochs with a batch size of 32, an LR of 1e-5, and two learning rate drops, once at 67% and the other at 89% of the total number of steps. AP scores are used in this case for model evaluation (Table C.1).

E Error Analysis

Although VoLTA learns impressive fine-grained region-level understanding during pre-training, there are still some cases where the model fails to identify tiny and hindered objects, especially in cluttered environments. We show four such examples in Figure E.1. In the first image, the object ‘red peppers’ is barely visible

Method	#Pre-train Data	VQAv2		NLVR ²		F30k IRTR		Method	#Pre-train Data	COCO Captioning											
		dev	std	dev	test-P	IR@1	TR@1			B@4	M	C	S								
<i>Models pre-trained on COCO (123k) and/or VG (108k)</i>																					
SCAN	108k	—	—	—	—	48.6	67.4	VL-T5	180k	34.5	28.7	116.5	21.9								
SCG	108k	—	—	—	—	49.3	71.8	VL-BART	180k	35.1	28.7	116.6	21.5								
PFAN	108k	—	—	—	—	50.4	70.0	Unified VLP	3M	36.5	28.4	117.7	21.3								
MaxEnt	123k	54.1	54.8	—	—	—	—	OSCAR	4M	36.5	30.3	123.7	23.1								
VisualBERT	123k	70.8	71.0	67.4	67.0	—	—	UFO-B	4M	36.0	28.9	122.8	22.2								
LXMERT	231k	72.4	72.5	74.9	74.5	—	—	ViTCAP	4M	36.3	29.3	125.2	22.6								
SOHO	231k	73.2	73.4	76.3	77.3	72.5	86.5	METER-CLIP-B	4M	38.8	30.0	128.2	23.0								
<i>Models pre-trained on COCO, VG, SBU (1M) and/or CC (3M)</i>																					
ViLBERT	3M	70.5	70.9	—	—	58.2	—	VinVL-B	4M	38.2	30.3	129.3	23.6								
UNITER-B	4M	72.7	72.9	77.2	77.9	72.5	85.9	XGPT	3.1M	37.2	28.6	120.1	21.8								
VILLA-B	4M	73.6	73.7	78.4	79.3	74.7	86.6	FIBER-B	4M	39.1	30.4	128.4	23.1								
UNIMO-B	4M	73.8	74.0	—	—	—	—	FIBER-GOLD-B	4M	40.3	30.7	133.6	23.6								
ViLT-B	4M	71.3	-	75.7	76.1	64.4	83.5	VoLTA-GOLD-B	231k	38.9	30.5	128.5	23.4								
ALBEF-B	4M	74.5	74.7	80.2	80.5	82.8	94.3	<i>Models fine-tuned with CIDEr optimization</i>													
VLMo-B	4M	76.6	76.9	82.8	83.3	79.3	92.3	ViTCAP	4M	41.2	30.1	138.1	24.1								
METER-Swin-B	4M	76.4	76.4	82.2	83.5	79.0	92.4	VinVL-B	4M	40.9	30.9	140.4	25.1								
FIBER-B	4M	78.6	78.4	84.6	85.5	81.4	92.9	FIBER-B	4M	42.8	31.0	142.8	24.3								
VoLTA-B	231k	74.6	74.6	76.7	78.1	72.7	83.6	FIBER-GOLD-B	4M	43.4	31.3	144.4	24.6								
								VoLTA-GOLD-B	231k	40.2	30.9	137.5	23.7								

Table F.1: **Multi-modal coarse-grained downstream: visual question answering, visual reasoning, retrieval, and captioning.** Methods pre-training with a significantly larger dataset are colored gray. For captioning, 4 metrics are reported - B@4: BLEU@4, M: METEOR, C: CIDEr, S: SPICE. The best comparable results are in **bold**. VoLTA-B denotes Swin-B backbone.

even in human eyes, and thus, VoLTA can not precisely identify these objects. However, it can identify the coarse region (the fruit basket) where ‘red peppers’ can be present. In the second image, VoLTA confuses a ‘dishwasher’ with a ‘microwave oven,’ probably because the ‘microwave oven’ is present in a cluttered environment, and both objects have similar appearances in low-resolution frames. In the third image, VoLTA can correctly identify ‘red apples’, but fails to spot ‘green apples’, probably because VoLTA has not seen enough such samples. In the last image, the face of the ‘person’ is hindered by the camera, and VoLTA fails to locate it. Since we pre-train VoLTA with 224×224 images, such tiny objects are often hard to be distinguished. However, higher-resolution images will be more helpful in addressing such intricate scenarios, which we plan to explore in future works.

F Additional Quantitative Results on Coarse-grained Vision-Language Tasks: Comparison with Methods using More Pre-training Data

Table F.1 presents a comparison of VoLTA on the multi-modal coarse-grained tasks with state-of-the-art methods pre-trained using magnitude more data. On VQA, VoLTA beats ViLBERT, UNITER-B, VILLA-B, UNIMO-B, and ViLT-B, each pre-trained on 3 – 4M datasets. Please note that VoLTA is trained only on COCO and VG, whereas the other methods use a combination of COCO, VG, CC, and SBU datasets. Such strong performance proves the generalizability of VoLTA. On captioning, VoLTA beats Unified VLP, OSCAR, UFO-B, ViTCAP, VinVL-B, METER-CLIP-B, and XGPT. However, for IRTR and NLVR VoLTA can not yield better performance over these baselines. We assume that the large domain difference between pre-training and downstream datasets is the reason behind the limited performance on IRTR and NLVR.

G Additional Qualitative Results

Visual Question Answering and Visual Reasoning: Visual question answering (VQA) is a widely recognized multi-modal task that infers an answer in response to a text-based question about an image. In Figure G.1, we demonstrated several examples image-question pairs and corresponding answers predicted by VoLTA on the VQAv2 validation set. The primary aim of the visual reasoning task is to ascertain the veracity of a natural language statement against an associated image pair. Figure G.2 displays examples of responses (True/False) predicted by VoLTA on the NLVR² validation set.

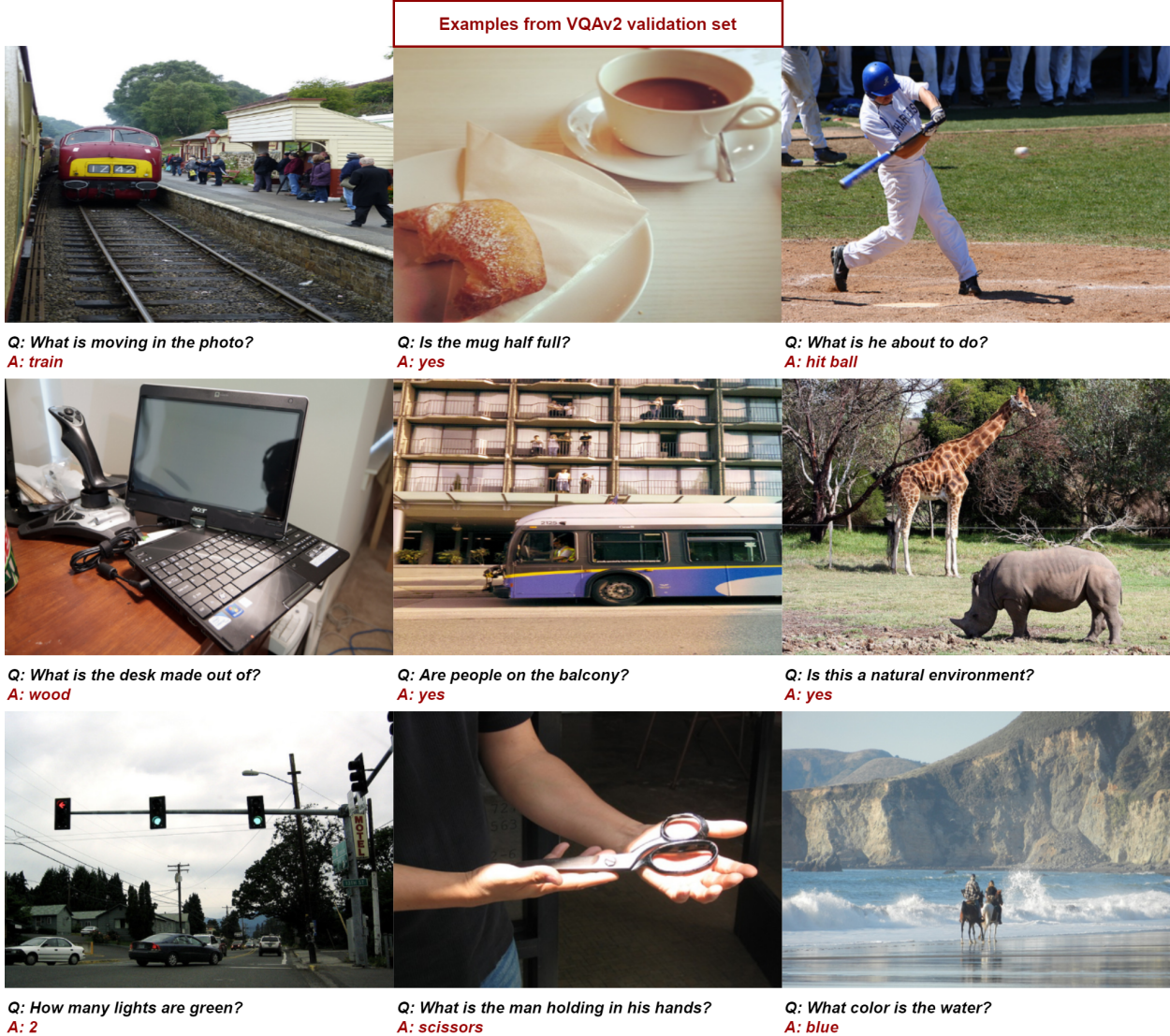


Figure G.1: **Examples on Visual Question Answering from VQAv2 validation dataset.** We display a variety of examples (e.g., number of items, the color of objects, type of objects, events, and actions) with respective answers predicted by VoLTA.

Language-conditioned Object Detection: Object detection forms an indispensable constituent of several multi-modal understanding systems. However, the conventional object detection pipeline is employed as a black-box tool and predicts all possible objects in the image. On the other hand, for better apprehension of combinations of these objects in free-form texts, a language-conditioned object detection task is considered (Kamath et al., 2021; Dou et al., 2022a). We use pre-trained VoLTA and fine-tuned and evaluated COCO and LVIS datasets for the text-conditioned object detection task. As illustrated in Figure G.3, VoLTA predicts bounding boxes relevant to the text prompts (captions) and labels them with the corresponding spans from the text. For example, the top-middle image has 4 objects. However, based on the text prompt, our model predicts boxes only for *person* and *cup*.

Referring Expression Comprehension (REC): The objective of REC is to align the entire referring expression (text) with the corresponding box by disambiguating among the several occurrences of an object belonging to the same category and therefore, one box per expression is to be predicted. For example, the bottom-left image in Figure G.4 depicts VoLTA’s box prediction for the corresponding referring expression: *the slice of cake on the left*.



Figure G.2: **Examples on Visual Reasoning from NLVR² validation dataset.** For each statement (text prompt), 2 images are shown alongside each other and VoLTA predicts whether the given statement is True (green box) or False (red box).

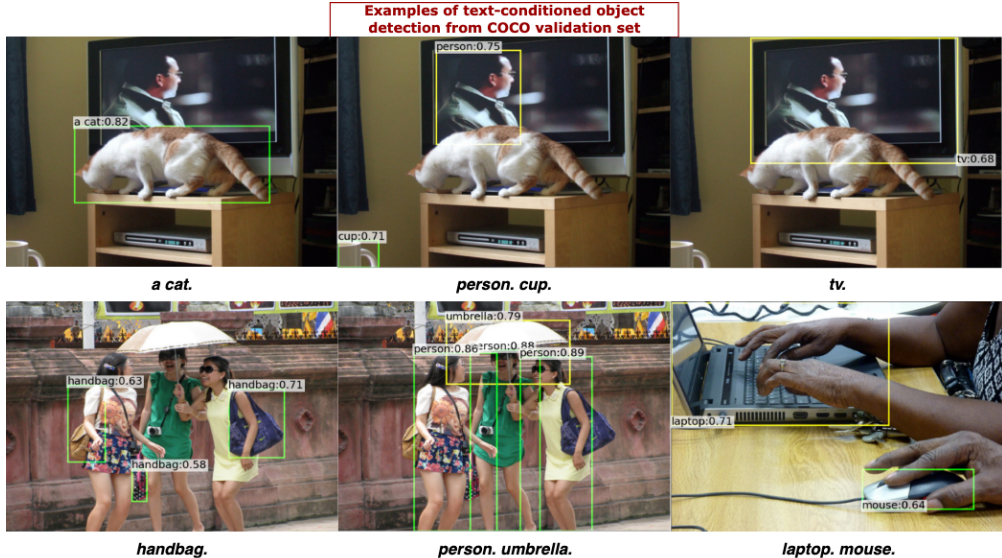


Figure G.3: **Examples of Object Detection from COCO validation dataset with various text prompts.** Our model predicts boxes relevant to the text (caption) and labels them with the corresponding spans.

Comparison of CLIP vs. VoLTA on Referring Expression Comprehension (REC): Figure G.5 shows a comparative qualitative evaluation between frozen CLIP + dynamic head (Dai et al., 2021), and VoLTA. We concatenate the vision and text features from the CLIP encoders and train a dynamic head on top of frozen features for the REC task. Since CLIP is a dual-encoder system pre-trained with image-level features, it can not learn superior fine-grained features. Hence, CLIP fails on harder REC samples. For example, if multiple similar-looking objects (benches or bowls) exist in an image, CLIP fails to distinguish between them. However, VoLTA succeeds on such complex samples, which can be attributed to the fine-grained alignment achieved by the GOT objective.

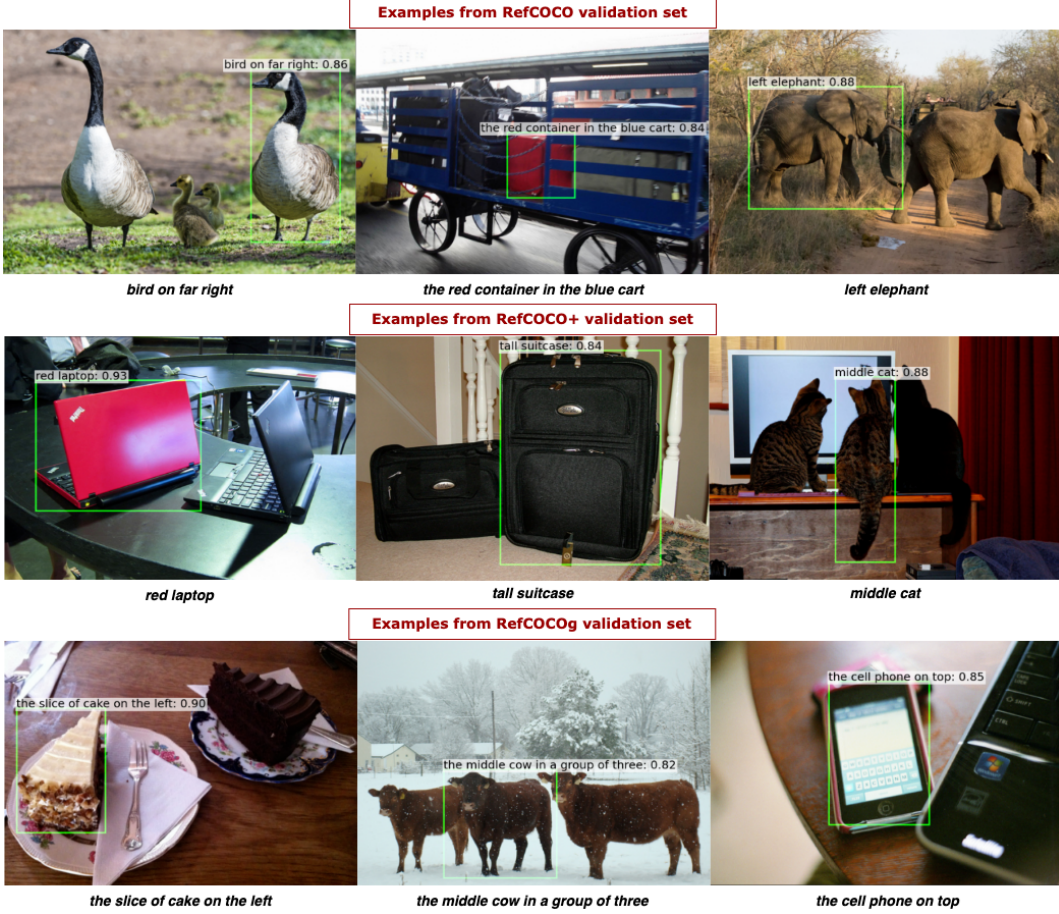


Figure G.4: Examples of Referring Expression Comprehension from RefCOCO (top), RefCOCO+ (middle) and RefCOCOg (bottom) validation datasets. The expressions in RefCOCOg typically have florid and longer constructions as compared to RefCOCO and RefCOCO+. The model has access to the entire text and uses it to disambiguate amongst different objects in the image.

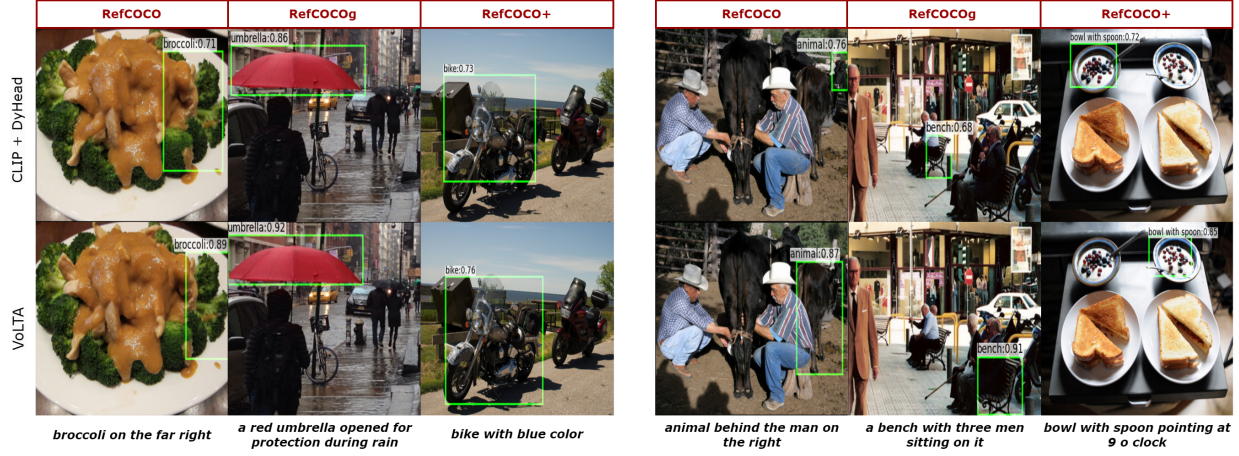


Figure G.5: Comparative qualitative evaluation between frozen CLIP + Dynamic Head (Dai et al., 2021), and VoLTA on different RefCOCO, RefCOCOg, RefCOCO+ validation samples.

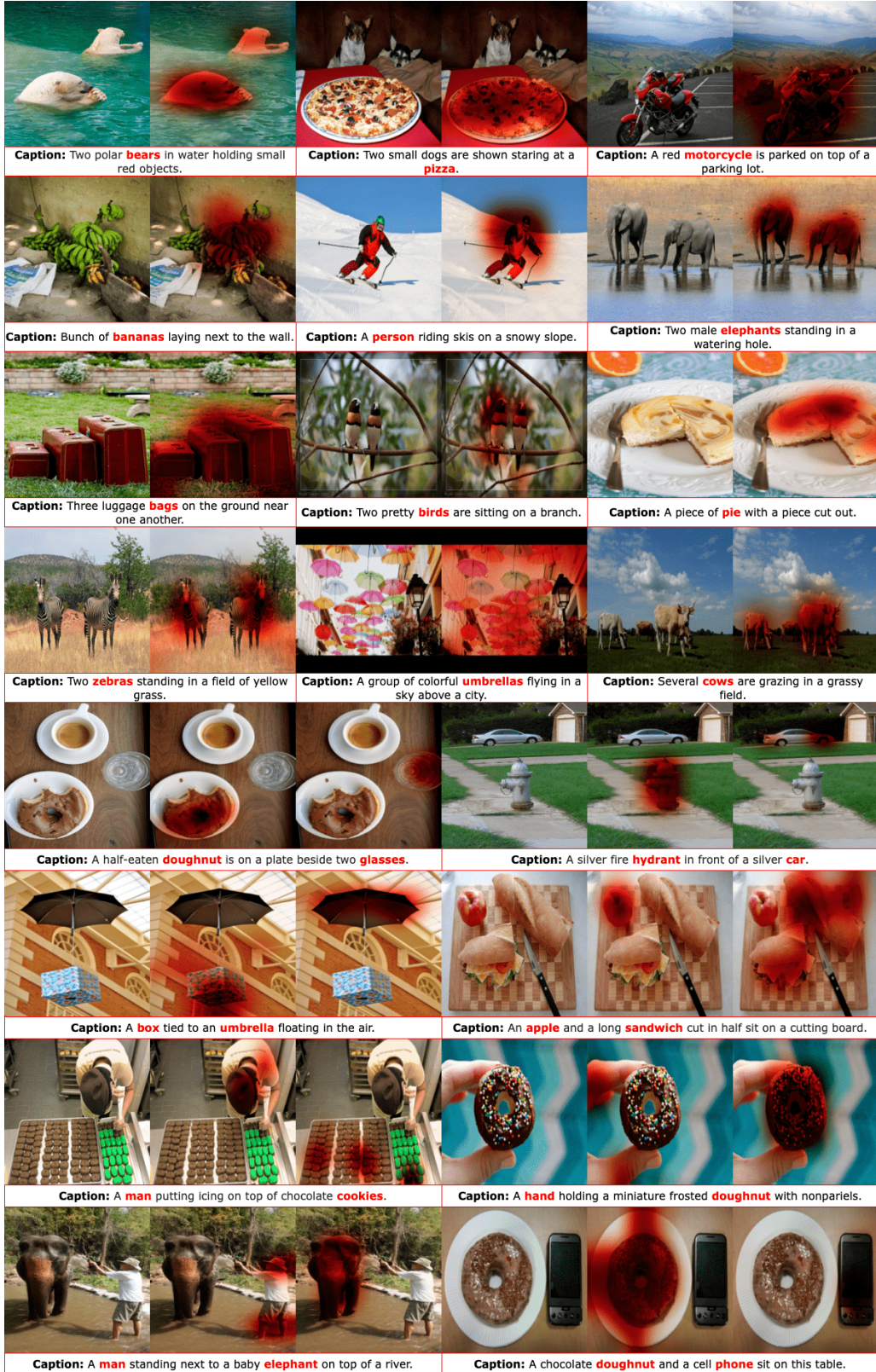


Figure G.6: This figure shows how different words in captions attend relevant image regions, produced by the GOT module of VOLTA pre-trained on COCO. Extension of Figure 4. All image-caption pairs are taken from the COCO2017 train split. The visualizations are generated with 224p images, resulting in sequences of 196 tokens for 16×16 patches.